Recurrent *FBXW7* mutations bypass Wnt/β-catenin addiction in cancer

Zheng Zhong[1], David M. Virshup[1,2,*]

[1]Program in Cancer and Stem Cell Biology, Duke-NUS Medical School, Singapore 169857

[2]Department of Pediatrics, Duke University, Durham, North Carolina, USA 27710

*** Corresponding author**

David M. Virshup

david.virshup@duke-nus.edu.sg

ORCID: 0000-0001-6976-850X

Duke-NUS Medical School, #07-20, 8 College Road, Singapore 169857

Running title: *FBXW7* mutations bypass Wnt addiction in cancer

Conflict of interest: David M. Virshup has a financial interest in ETC-159.

Abstract

Pathologic Wnt/β-catenin signaling drives various cancers, leading to multiple approaches to drug this pathway. Appropriate patient selection can maximize success of these interventions. Wnt ligand addiction is a druggable vulnerability in *RNF43*-mutant/*RSPO*-fusion cancers. However, pharmacologically targeting the biogenesis of Wnt ligands, e.g., with PORCN inhibitors, has shown mixed therapeutic responses, possibly due to tumor heterogeneity. Here we show that the tumor suppressor *FBXW7* is frequently mutated in *RNF43*-mutant/*RSPO*-fusion tumors, and *FBXW7* mutations cause intrinsic resistance to anti-Wnt therapies. Mechanistically, inactivation of FBXW7 stabilizes multiple oncoproteins including Cyclin E and MYC, and antagonizes the cytostatic effect of Wnt inhibitors. Moreover, although *FBXW7* mutations do not mitigate β-catenin degradation upon Wnt inhibition, *FBXW7*-mutant *RNF43*-mutant/*RSPO*-fusion cancers instead lose dependence on β-catenin signaling, accompanied by dedifferentiation and loss of lineage specificity. These *FBXW7*-mutant Wnt/β-catenin-independent tumors are susceptible to multi-CDK inhibition by dinaciclib. An in depth understanding of primary resistance to anti-Wnt/β-catenin therapies allows for more appropriate patient selection and use of alternative mechanism-based therapies.

Introduction

Active Wnt signaling maintains the stem cell populations in multiple adult tissues while its hyperactivation due to genetic alterations drives many human cancers[1,2]. Canonical Wnt signaling is activated by the engagement of secreted Wnt ligands with cell surface receptors Frizzleds (FZDs) and LRP5/6, leading to inactivation of GSK3 and stabilization of the transcriptional regulator β-catenin and other effector proteins such as MYC. Two categories of genetic events activate the Wnt pathway in human cancers: (1) downstream mutations, e.g., *APC* truncating mutations or *CTNNB1* (β-catenin) degron site mutations, that dissociate β-catenin regulation from upstream signaling and lead to its constitutive stabilization and activation; (2) mutations in the upstream regulators of Wnt receptors, such as inactivating mutations in the FZD-targeting E3 ubiquitin ligase genes *RNF43*/*ZNRF3* or gene fusions involving *RSPO2*/*3* leading to R-spondin overexpression that inactivates RNF43/ZNRF3[3,4]. Both *RNF43*/*ZNRF3* mutations and *RSPO2*/*3* fusions up-regulate cell surface abundance of Wnt receptors and hypersensitize cells to Wnt ligands. These upstream mutations can be detected in diverse gastrointestinal cancers, e.g., *RNF43* mutations are present in 5-10% pancreatic cancers and *RSPO2*/*3* fusions are found in 2-10% colorectal cancers[4–9].

Notably, while it remains challenging to therapeutically target stabilized β-catenin in cancers, the *RNF43*-mutant/*RSPO*-fusion cancers are attractive because preclinical studies revealed that multiple cancers with these molecular lesions are hypersensitive to upstream Wnt signaling blockade. Multiple modalities have been developed to achieve this and have had preclinical successes[3,10,11]. These include targeting the biogenesis of Wnt ligands with small molecule PORCN inhibitors[3,10], blocking the interaction between Wnt ligands and receptors using anti-FZD antibodies or recombinant Wnt decoy receptors[12–14], and targeting R-spondins using RSPO2/3-neutralizing antibodies[11,15]. Most notably, several PORCN inhibitors are being actively investigated in clinical trials, and it is anticipated that patient selection will be driven at least in part by these biomarkers[1].

Notably, the therapeutic response to PORCN inhibitors is heterogeneous in *RNF43*-mutant/*RSPO*-fusion cancer patients[16,17]. On one hand, durable responses were observed in several patients, confirming the important role of Wnt addiction and supporting the potential clinical benefits of PORCN inhibitors. On the other hand, intrinsic or acquired drug resistance was frequently observed during PORCN inhibitor treatment. However, the underlying mechanisms for PORCN inhibitor resistance remain elusive.

To identify potential drug resistance mechanisms, we previously performed an *in vivo* CRISPR gene knockout screen during PORCN inhibitor treatment in mice bearing *RNF43*-mutant pancreatic cancer xenografts. This screen identified gene candidates whose loss could cause Wnt independence and led to the discovery that defects in the p300/GATA6/differentiation axis can bypass the anti-differentiation role of Wnt signaling specifically in pancreatic cancer[18]. However, this does not appear to explain the drug resistance observed in those non-pancreatic cancer models, most notably in colorectal cancers. In the current study, we comprehensively investigate another hit from the screen, *FBXW7*, that encodes the substrate recognition component of a SCF E3 ubiquitin ligase complex. We find that *FBXW7* is frequently mutated in *RNF43*-mutant/*RSPO*-fusion cancers regardless of the tissue of origin. Inactivation of FBXW7 causes intrinsic resistance to Wnt inhibition by stabilizing oncoproteins including MYC and Cyclin E. Interestingly, *FBXW7* mutants lose dependence on β-catenin, accompanied by dedifferentiation and loss of lineage specificity, suggesting a cancer evolutionary trajectory from Wnt-dependent low-grade tumors to Wnt-independent and dedifferentiated cancers. *FBXW7* mutations may be a powerful biomarker for patient selection, as they may drive a major drug resistance mechanism limiting the effectiveness of diverse therapies targeting Wnt/β-catenin signaling.

Results

Recurrent *FBXW7* mutations in *RNF43*-mutant/*RSPO*-fusion cancers

Our previous *in vivo* CRISPR screen identified several genes whose knockout caused resistance to a PORCN inhibitor[18]. Most of these genes are known negative regulators of Wnt pathway, e.g., *APC* and *AXIN1*, so that their knockout provides downstream activation of Wnt/β-catenin signaling. These genes were independently observed in a genome-wide *in vitro* screen performed by the Angers group aiming to find resistance genes against another PORCN inhibitor[19]. One unexpected hit from both screens was *FBXW7*, a known tumor suppressor but one that is not obviously involved in regulating Wnt signaling[20]. To study how alterations in these putative resistance genes might affect the overall clinical response of Wnt-targeting therapies, we analyzed their mutation frequency in *RNF43*-mutant/*RSPO*-fusion cancers. We focused on all types of genetic alterations of *FBXW7* and established Wnt/β-catenin-activating mutations including *APC* or *AXIN1* truncation/deletion and *CTNNB1* stabilizing missense mutations.

96 In a combined cohort of colorectal cancers harboring *PTPRK-RSPO3* fusions, the most
97 common *RSPO*-fusion cancer type, *FBXW7* mutations were detected in 25% cases (**Fig. 1A**).
98 Half of these *FBXW7* mutations were hotspot missense mutations that are known to be
99 dominant-negative. Truncations of *FBXW7*, that are presumably inactivating, were also
100 common. This mutational landscape is similar to the *FBXW7* mutation landscape in the bulk
101 of colorectal cancers, largely due to *APC* mutations[20]. In contrast, mutations in *APC*, *AXIN1*,
102 and *CTNNB1* were very rare in *RSPO*-fusion colorectal cancers, as only one *APC* truncation
103 was detected (**Fig. 1A**).

104 *RNF43* mutations appear in multiple cancer types, so we performed a pan-cancer analysis
105 of *RNF43* and those putative drug resistance genes (**Fig. 1B**). As the role of the recurrent
106 *RNF43* G659 microsatellite-related frameshift mutations remains controversial[21–24], we
107 analyzed those separately from the non-G659-related truncations. For missense mutations of
108 *RNF43*, we annotated them based on previous characterization studies[23,25] and classified them
109 as driver mutations (loss of function, partial loss of function, or dominant-negative) or
110 mutations of unknown significance. Cancer cases with known benign missense mutations in
111 *RNF43* were excluded. Importantly, *FBXW7* mutations were detected in 16.7% of all *RNF43*-
112 mutant cancers. Again, around half of these *FBXW7* alterations were hotspot missense
113 mutations. Notably, different from *RSPO*-fusion colorectal cancers, a significant subset (17.8%)
114 of *RNF43*-mutant cancers harbored downstream β-catenin-stabilizing mutations in either *APC*,
115 *AXIN1*, or *CTNNB1*.

116 In summary, we identified recurrent *FBXW7* mutations in 16-25% of both *RNF43*-mutant
117 and *RSPO3*-fusion cancers. In *RNF43*-mutant cancers, we also observed frequent *APC*, *AXIN1*,
118 or *CTNNB1* mutations that stabilize and activate β-catenin. These mutations could result in
119 resistance to anti-Wnt therapies in *RNF43*-mutant/*RSPO3*-fusion cancers.

120 ***FBXW7* mutation status predicts resistance to Wnt inhibition**

121 To evaluate if pre-existing *FBXW7* mutations predicted resistance to anti-Wnt therapies,
122 we collected a panel of cancer cell lines from diverse lineages harboring inactivating mutations
123 in *RNF43*/*ZNRF3* or *RSPO2*/*3* fusions and tested their response to the PORCN inhibitor ETC-
124 159 in a soft agar colony formation assay (**Fig. 2A**). As previously reported[3,26,27], HPAF-II and
125 other cell lines without other Wnt pathway mutations failed to form colonies in the presence
126 of the PORCN inhibitor. As expected, HuG1-N and HCT116, the two cell lines with additional
127 APC truncation and β-catenin-stabilizing mutation, respectively, were resistant to ETC-159.

128 Importantly, the three cell lines harboring *FBXW7* mutations, AsPC-1 and NCIH2172 with
129 hotspot mutations and HuCCT1 with a truncating mutation, were either less sensitive or highly
130 resistant to ETC-159.

131 To test if these *FBXW7* mutations affected drug sensitivity *in vivo*, we examined the growth
132 inhibition efficacy of ETC-159 in mouse xenografts of three pancreatobiliary cancer cell lines
133 with *RNF43* mutations (**Fig. 2B**). Consistent with the *in vitro* observation, while ETC-159
134 potently suppressed the *FBXW7*-wildtype HPAF-II tumor growth, at the same dose the AsPC-
135 1 tumor had only 30% tumor growth inhibition, and there was no effect on the HuCCT1 tumor.

136 In a preclinical study from OncoMed using an RSPO3-neutralizing antibody to treat
137 *RSPO3*-fusion colorectal cancers[15], three of four *RSPO3*-fusion positive patient-derived
138 xenografts (PDXs) showed tumor growth inhibition, while a fourth tumor, CR1560, was
139 unaffected. We speculated that this resistance could be due to a pre-existing *FBXW7* mutation.
140 Indeed, inspection of mutation profiles of these four PDXs revealed a hotspot p.R465C
141 mutation of *FBXW7* only in the drug resistant PDX (**Fig. 2C**). Moreover, in these PDXs and
142 the above tested cancer cell lines, the sensitivity to anti-Wnt therapies was not related to the
143 other oncogenic driver mutations including alterations in *KRAS*, *BRAF*, *TP53*, and *SMAD4*
144 (**Fig. 2A** and **C**). These results, taken together, suggest that pre-existing *FBXW7* mutations are
145 common in *RNF43*-mutant/*RSPO3*-fusion cancers and cause resistance to Wnt inhibitors.

146 Wnt inhibition leads to cell cycle arrest and differentiation rather than cell death in Wnt-
147 addicted cancers[14,18,26,28]. We examined if the molecular response to anti-Wnt therapies differed
148 in the *FBXW7*-wildtype versus mutant tumors (**Fig. 2D**). In the *FBXW7*-wildtype HPAF-II
149 xenografts, PORCN inhibition led to significant dephosphorylation of Rb protein and (as
150 dephosphorylated Rb is less stable[29,30]) reduced total Rb abundance. PORCN inhibition also
151 markedly reduced the abundance of E2F1, a key regulator of the cell cycle progression. These
152 indicate a potent cell cycle arrest in HPAF-II tumors, consistent with our prior studies[28]. In
153 contrast, these effects were largely attenuated or even absent in the *FBXW7*-mutant AsPC-1
154 and HuCCT1 tumors (**Fig. 2D**). Similar results were noted when we reanalyzed the data from
155 the OncoMed study of *RSPO3*-fusion colorectal cancer PDXs[15], where the RSPO3-neutralizing
156 antibody treatment led to potent cell cycle arrest in the three sensitive models but showed no
157 effect in the *FBXW7*-mutant drug resistant PDX (**Fig. 2E**). Therefore, the association of
158 *FBXW7* mutations and PORCN inhibitor resistance was confirmed on the molecular level in
159 both *RNF43*-mutant and *RSPO*-fusion cancers.

160 Taken together, these results establish a strong correlation between *FBXW7* mutations and
161 resistance to anti-Wnt therapies in *RNF43*-mutant/*RSPO*-fusion cancers. These also suggest
162 that *FBXW7* mutation status can be used as a biomarker for patient selection for anti-Wnt
163 therapies.

164 **Inactivation of FBXW7 confers intrinsic resistance to Wnt inhibition**

165 To directly test if *FBXW7* mutations cause the drug resistance and to study the underlying
166 mechanism, we inactivated *FBXW7* in PORCN inhibitor-sensitive cancer cells and examined
167 if they became inhibitor resistant. Specifically, we truncated the endogenous FBXW7 protein
168 approximately at amino acid position 420 in the *FBXW7*-wildtype *RNF43*-mutant HPAF-II
169 pancreatic cancer cells using CRISPR/Cas9 (**Fig. S1**) and subsequently tested the sensitivity of
170 the xenografts to PORCN inhibitor ETC-159 (**Fig. 3A**). Notably, immediately after initiation
171 of this animal study, Singapore entered the unexpected COVID-19 lockdown period, during
172 which time we only had limited access to the vivarium. Therefore, these tumor-bearing mice
173 were treated with an intermittent drug dosing schedule that nevertheless produced a significant
174 tumor growth inhibition in control tumors (**Fig. 3A**, left). In contrast, ETC-159 had no effect
175 on the growth of tumors with FBXW7 truncations (**Fig. 3A**, right).

176 Half of the *FBXW7* mutations detected in clinical samples are hotspot missense mutations
177 that known to be dominant-negative[20] (**Fig. 1**). To examine the effect of these dominant-
178 negative mutations on drug resistance, we stably expressed an exogenous FBXW7 p.R465C
179 hotspot mutant in *FBXW7*-wildtype *RSPO3*-fusion SNU1411 colorectal cancer cells (**Fig. 3B**).
180 Similar to the truncation mutants, while ETC-159 inhibited growth of the parental SNU1411
181 xenografts in a dose-dependent manner, the growth of tumors expressing the FBXW7 dominant
182 negative mutant no longer responded to ETC-159 treatment (**Fig. 3B**). Taken together, these
183 results demonstrate that inactivation of FBXW7 through either truncations or dominant-
184 negative missense mutations confers intrinsic resistance to Wnt inhibition in *RNF43*-
185 mutant/*RSPO*-fusion cancers.

186 **FBXW7 mutations function in part by stabilizing MYC and Cyclin E**

187 We next investigated the molecular mechanisms underlying the drug resistance caused by
188 FBXW7 inactivation. Previously we showed that in drug-sensitive *RNF43*-mutant/*RSPO*-
189 fusion tumors Wnt inhibition down-regulated the cell cycle machinery due to suppression of
190 the Wnt/β-catenin/MYC network[28], and this led to a potent cell cycle arrest. As the substrate
191 recognition subunit of a SCF E3 ubiquitin ligase complex, FBXW7 controls the degradation of

192 multiple oncoproteins[20,31]. We hypothesized that inactivation of FBXW7 leads to the
193 accumulation or prevents the degradation of certain proteins that antagonize the cytostatic
194 effect of Wnt inhibitors. We therefore examined the protein abundance of various known
195 FBXW7 substrates in the HPAF-II and SNU1411 xenograft tumors treated with or without
196 ETC-159. Out of the six reported FBXW7 substrates (**Fig. 4A**), we observed consistent up-
197 regulation of Cyclin E1 in both HPAF-II and SNU1411 tumors after FBXW7 inactivation. In
198 HPAF-II tumors, FBXW7 inactivation increased basal MYC abundance, while this effect was
199 less evident in SNU1411 tumors. However, in both models, FBXW7 inactivation mitigated the
200 degradation of MYC upon ETC-159 treatment (**Fig. 4A**). This was due to increased MYC
201 stability after FBXW7 inactivation (**Fig. S2**). Other known FBXW7 substrates were regulated
202 in a context-dependent manner, as we observed an increase in KLF5 abundance after FBXW7
203 inactivation in HPAF-II tumors, and an increase in PKM2 abundance only in SNU1411 tumors
204 (**Fig. 4A**). Two other presumed FBXW7 substrates, c-Jun and the NOTCH1 intracellular
205 domain, were not affected in either model.

206 Stabilization of Cyclin E1 and MYC by FBXW7 inactivation was consistently observed in
207 two independent models. To test whether these proteins mediated the FBXW7 inactivation-
208 caused drug resistance, we ectopically expressed human mutant Cyclin E1 and/or MYC in
209 HPAF-II cells (**Fig. 4B**). These mutants cannot be phosphorylated by GSK3 and so they cannot
210 be subsequently recognized by FBXW7. Notably, expressing either mutant Cyclin E or mutant
211 MYC led to a clear shift of the ETC-159 dose-response curve in the soft agar colony formation
212 assay (**Fig. 4C**), reflecting drug resistance. Interestingly, co-expressing stabilized Cyclin E and
213 MYC only modestly further enhanced the drug resistance (**Fig. 4C**), suggesting that Cyclin E
214 and MYC might share redundant roles in this setting. This is consistent with the observation
215 that expressing mutant MYC alone also up-regulated Cyclin E abundance (**Fig. 4B**). Thus,
216 FBXW7 inactivation causes intrinsic resistance to Wnt inhibition at least partially due to
217 stabilization of Cyclin E and MYC.

218 We extended this observation to the naturally pre-existing *FBXW7*-mutant drug resistant
219 models. For example, the *FBXW7*-mutant AsPC-1 tumors had a significantly higher Cyclin E1
220 protein (but not mRNA) abundance than the *FBXW7*-wildtype HPAF-II tumors (**Fig. 4D** and
221 **Fig. S3**). Moreover, in both *FBXW7*-mutant AsPC-1 and HuCCT1 tumors, ETC-159 treatment
222 no longer led to a significant decrease of MYC protein (**Fig. 4D**). This is consistent with our
223 reanalysis of the transcriptomic response data reported in the *RSPO3*-fusion colorectal cancer
224 PDXs[15], where treatment with RSPO3-neutralizing antibody significantly down-regulated the

225 mRNA levels of MYC target genes in all the models except CR1560 bearing a hotspot *FBXW7*
226 mutation (**Fig. 4E**). The above findings demonstrate that inactivation of FBXW7 confers
227 intrinsic resistance to Wnt inhibition in *RNF43*-mutant/*RSPO*-fusion cancers at least in part
228 through stabilizing MYC and Cyclin E.

229 ***FBXW7*-mutant *RNF43*-mutant/*RSPO*-fusion cancers lose their dependence on β-catenin**
230 **signaling**

231 *RNF43*-mutant/*RSPO*-fusion cancers are addicted to β-catenin signaling[3]. The resistance
232 conferred by *FBXW7* mutations functions through stabilization of MYC and Cyclin E. Because
233 β-catenin is regulated by a different E3 ubiquitin ligase that uses β-TrCP as a substrate
234 recognition subunit[32], *FBXW7* mutations should have no effect on β-catenin degradation upon
235 Wnt inhibition (**Fig. 5A**). This raised an interesting question – was β-catenin stable in *FBXW7*-
236 mutant cancers, or did the *FBXW7*-mutant cancers no longer rely on β-catenin?

237 To test if FBXW7 inactivation affects β-catenin degradation upon Wnt inhibition, we used
238 immunohistochemistry to examine β-catenin abundance in the *RSPO3*-fusion SNU1411
239 colorectal tumor models. As expected, the basal β-catenin level was high in both cytoplasm
240 and nucleus of the xenograft tumors, and PORCN inhibition robustly reduced β-catenin
241 abundance (**Fig. 5B**). Importantly, the reduction of β-catenin was similarly observed in
242 xenografts that expressed the dominant-negative FBXW7 mutant (**Fig. 5B**), confirming that
243 inactivation of FBXW7 does not mitigate β-catenin degradation. Since these *FBXW7*-mutant
244 SNU1411 tumors continued growing during ETC-159 treatment (**Fig. 3B**), they must have lost
245 their initial dependence on β-catenin. We extended this observation in additional *RNF43*-
246 mutant tumor xenografts. As expected, *FBXW7*-wildtype tumors had high basal levels of β-
247 catenin that significantly decreased after Wnt inhibition (**Fig 5C**, left). Notably, the *FBXW7*-
248 mutant tumors showed lower levels of β-catenin in both the cytoplasm and nucleus even
249 without ETC-159 treatment (**Fig. 5C**, right). These observations suggest that during cancer
250 evolution *RNF43*-mutant/*RSPO*-fusion cancer cells lose their dependence on Wnt/β-catenin
251 after acquiring *FBXW7* mutations.

252 To test if β-catenin indeed becomes dispensable, we explored the specific requirements for
253 β-catenin and MYC in *FBXW7* wildtype and mutant xenograft tumors. We used a dCas9-
254 KRAB-mediated gene knockdown system where the expression of sgRNAs targeting the
255 *CTNNB1* or *MYC* promoters could be induced by doxycycline treatment. As expected,
256 knockdown of β-catenin in the Wnt-dependent HPAF-II cells potently suppressed tumor
257 growth (**Fig. 6A** and **B**). As *MYC* is a β-catenin target gene, β-catenin knockdown in HPAF-II

258 cells partially reduced *MYC* mRNA abundance (**Fig. 6A**). In contrast, direct knockdown of
259 *MYC* transcription had a much smaller effect on HPAF-II tumor growth and did not phenocopy
260 the tumor growth inhibition caused by β-catenin knockdown (**Fig. 6A** and **B**). This is consistent
261 with our understanding that in Wnt-addicted cancers β-catenin plays more roles besides
262 transcriptionally regulating *MYC* expression[28].

263 In sharp contrast, in the *RNF43*-deleted but *FBXW7*-mutant HuCCT1 xenografts, depleting
264 β-catenin no longer affected *MYC* transcription nor tumor growth (**Fig. 6C** and **D**). Instead,
265 knockdown of *MYC* potently inhibited HuCCT1 tumor growth (**Fig. 6D**), suggesting that these
266 *FBXW7*-mutant cancer cells had lost dependence on β-catenin and had shifted their oncogene
267 addiction to MYC. Moreover, β-catenin knockdown did not affect the spontaneous lung
268 metastasis occurred in HuCCT1 xenograft-bearing mice. Histopathologic analysis confirmed
269 that cancer cells of the lung metastases were highly proliferative despite the absence of β-
270 catenin (**Fig. 6E**), confirming that β-catenin is dispensable in this model. Similarly, we knocked
271 down β-catenin in AsPC-1 xenografts that harbor a *FBXW7* mutation but partially responded
272 to Wnt inhibition. We speculate that these tumors may represent a transition state towards
273 Wnt/β-catenin independence. β-catenin knockdown delayed initial AsPC-1 tumor growth, but
274 after a period of adaptation these tumors grew as fast as control (**Fig. S4A**). As with the
275 HuCCT1 tumors, *MYC* transcription was no longer affected by β-catenin knockdown in these
276 AsPC-1 xenograft tumors (**Fig. S4B**), consistent with the loss of β-catenin dependence. In
277 summary, the data indicate that FBXW7 is not directly involved in the Wnt/β-catenin axis, but
278 that *RNF43*-mutant/*RSPO*-fusion cancers lose their dependence on β-catenin signaling after
279 acquiring *FBXW7* mutations.

280 **Inactivation of FBXW7 leads to dedifferentiation and phenotypic switching in *RNF43*-**
281 **mutant/*RSPO*-fusion cancers**

282 Hyperactivated Wnt/β-catenin signaling in *RNF43*-mutant/*RSPO*-fusion tumors maintains
283 cancer stemness, while Wnt inhibition promotes cancer cell differentiation[10,11,18]. Since
284 *FBXW7*-mutant *RNF43*-mutant/*RSPO*-fusion cancers have low levels of β-catenin (**Fig. 5C**),
285 we speculated that these cancers might be more differentiated. However, while cancer cells in
286 the *FBXW7*-wildtype HPAF-II tumors formed large glandular-like epithelial structures,
287 reflecting a well/moderately differentiated state, these structures were rarely seen in the
288 *FBXW7*-mutant tumors (**Fig. 7A**). Consistent with a more mesenchymal phenotype, these
289 *FBXW7*-mutant cancer cells have low expression of the epithelial marker E-cadherin and high
290 expression of the mesenchymal marker vimentin (**Fig. S5**). We further examined the expression

291 of mucin as a marker of differentiation in these xenografts. The *FBXW7*-mutant tumors showed
292 comparable if not less mucin staining compared with the *FBXW7*-wildtype HPAF-II tumors
293 (**Fig. 7A**). Notably, while Wnt inhibition significantly promoted mucin expression in HPAF-II
294 tumors, it had no effect in the two *FBXW7*-mutant cancers (**Fig. 7A**). In conclusion, *FBXW7*-
295 mutant *RNF43*-mutant/*RSPO*-fusion tumors appeared to be less differentiated and are
296 refractory to the Wnt inhibition-induced differentiation program.

297 Pancreatic cancers are classified into two major subtypes, a well/moderately differentiated
298 classical subtype and a poorly differentiated basal-like/squamous subtype[6,33–35]. Our previous
299 work showed that active Wnt/β-catenin signaling is present in the classical rather than the
300 basal-like/squamous subtype[18]. Indeed, *RNF43*-mutant pancreatic tumors are enriched in the
301 classical subtype[7,18]. Consistent with this, the *FBXW7*-wildtype HPAF-II tumors showed clear
302 classical subtype features[18]. However, the *FBXW7*-mutant AsPC-1 tumors showed a more
303 mesenchymal phenotype (**Fig. 7A** and **Fig. S4**), a key feature of the basal-like subtype. This
304 suggested a role of *FBXW7* mutation in mediating the subtype transition. To examine if
305 changes in FBXW7 caused the subtype transition, we analyzed the expression of several
306 subtype-related marker genes in HPAF-II tumors after FBXW7 truncation (**Fig. 7B**). Indeed,
307 FBXW7 inactivation down-regulated the expression of the classical subtype genes and up-
308 regulated the basal-like subtype genes. Interestingly, FBXW7 inactivation also down-regulated
309 the expression of several well-established Wnt/β-catenin target genes (**Fig. 7B**), consistent with
310 our previous finding that pancreatic basal-like subtype tumors have low β-catenin signaling[18].
311 In summary, inactivation of FBXW7 in *RNF43*-mutant pancreatic cancers leads to subtype
312 switching.

313 Similarly, recent studies have divided colorectal cancer cells into two distinct cancer cell
314 states[36–38]. One state has high LGR5+ adult intestinal stemness markers and is commonly
315 observed in the CMS2 subtype of colorectal tumors that show high Wnt/β-catenin signaling
316 and epithelial differentiation. The other state features a fetal-like and regenerative intestinal
317 gene signature and is associated with tumors that have low Wnt/β-catenin signaling and
318 mesenchymal phenotype. We found that inactivating FBXW7 by expressing a dominant-
319 negative mutant in the *RSPO3*-fusion colorectal SNU1411 tumors up-regulated the expression
320 of fetal-like colorectal cancer markers (**Fig. 7B**). Moreover, among the *RSPO3*-fusion
321 colorectal cancer PDXs, the PDX harboring a *FBXW7* hotspot mutation also highly expressed
322 the fetal-like tumor markers while had low expression of the LGR5+ stemness markers (**Fig.
323 7C**). These results suggest that inactivation of FBXW7 in *RSPO*-fusion colorectal cancers also

leads to a subtype switching. We even noted a marked decrease of the expression of intestinal lineage markers in the *FBXW7*-mutant PDX (**Fig. 7C**), reflecting a dedifferentiated status that lacks lineage specificity.

In summary, inactivation of FBXW7 in *RNF43*-mutant/*RSPO*-fusion cancers leads to cancer cell dedifferentiation and a phenotypic switch from a Wnt-high epithelial state to a Wnt-low mesenchymal state. Previously we showed in pancreatic cancer that the classical subtype tumors require active Wnt/β-catenin signaling to antagonize the differentiation program, while the basal-like subtype tumors intrinsically inactivated the differentiation program and therefore lost β-catenin dependence[18]. Similarly, the dedifferentiated *FBXW7*-mutant tumors no longer require active Wnt/β-catenin signaling to prevent differentiation and therefore are resistant to Wnt inhibition-induced differentiation (**Fig. 7A**).

***FBXW7*-mutant cancers are sensitive to multi-CDK inhibition**

FBXW7 mutations in *RNF43*-mutant/*RSPO*-fusion cancers lead to loss of Wnt dependence and drug resistance to anti-Wnt therapies. We examined if there are alternative strategies to treat these *FBXW7*-mutant cancers. As shown previously, Cyclin E and MYC proteins were stabilized in these *FBXW7*-mutant cancer cells and were functionally important. While it remains challenging to therapeutically target MYC directly, Cyclin E's function can be targeted using small molecule inhibitors of the Cyclin E-coupled kinase, CDK2. As MYC may act as a general amplifier that globally enhances transcription[39,40], an alternative strategy of targeting MYC activity in cancer is to down-regulate the hyperactivated transcription program directly, e.g., through inhibiting the activity of transcription-associated CDKs[41]. Therefore, the goal of simultaneously targeting the Cyclin E/CDK2-driven cell cycle progression and the MYC-driven transcription in *FBXW7*-mutant cancers could be achieved by multi-CDK inhibitor treatment. To test this, we treated two *FBXW7*-mutant cancer xenograft models with the multi-CDK inhibitor dinaciclib that targets both the cell cycle-associated CDK1/2 and the transcription-associated CDK9/12[42,43]. As a proof of concept, low-dose dinaciclib treatment significantly suppressed tumor growth in both models (**Fig. 8A**), reflecting their high sensitivity to anti-cell cycle/transcription treatment. While the dinaciclib-treated tumors were still slowly growing, perhaps due to the short *in vivo* half-life of dinaciclib (murine plasma half-life of ~0.25 hour[42]) and low dosing frequency, these results reveal the potential of treating *FBXW7*-mutant cancers with multi-CDK inhibitors such as dinaciclib.

355 ## Discussion

356 Hyperactivated Wnt signaling is a potent driver of diverse human cancers, but no drug
357 targeting the Wnt pathway has been approved for cancer therapy so far[1]. The discovery of
358 specific *RNF43* mutations and *RSPO* fusions that caused addiction to upstream Wnt signaling
359 in *RNF43*-mutant/*RSPO*-fusion cancers, coupled with the development of clinically tolerated
360 upstream Wnt pathway inhibitors has generated cautious optimism for anti-Wnt therapies.
361 However, even within this genetically defined *RNF43*-mutant/*RSPO*-fusion cancer cohort, pre-
362 existing drug resistance represents a significant patient selection problem[16,17]. In this study, we
363 identified recurrent *FBXW7* mutations in *RNF43*-mutant/*RSPO*-fusion cancers and
364 demonstrated that this is a major drug resistance mechanism.

365 In *RNF43*-mutant/*RSPO*-fusion cancers, a Wnt/β-catenin/MYC network maintains the
366 active cell cycle[28], and therefore Wnt inhibition causes cell cycle arrest followed by senescence.
367 *FBXW7* mutations stabilize Cyclin E and MYC proteins to antagonize the cytostatic effect of
368 Wnt inhibitors and therefore cause drug resistance (**Fig. 8B**). This is consistent with the finding
369 that overexpression of Cyclin E or MYC in multiple other cancers, frequently due to gene
370 amplification, is an important mechanism that confers resistance to targeted cytostatic agents,
371 e.g., CDK4/6 inhibitors and certain tyrosine kinase inhibitors[44–49]. Notably, there might be
372 other substrates not examined in our study that also contributed to cell cycle progression after
373 *FBXW7* mutation. For example, another cell cycle regulator Cyclin L1 was recently identified
374 as a novel substrate of FBXW7 and accumulated in FBXW7-inactivated cells[19]. Elevated levels
375 of Cyclin L1 might also help to maintain the active cell cycle during Wnt inhibition.

376 An unexpected finding in our study that has broad implications is the loss of β-catenin
377 dependence in these Wnt/β-catenin-driven cancers after gaining *FBXW7* mutations. We
378 attempted to interpret this observation based on a simplified model where upstream Wnt
379 signaling stabilizes two groups of GSK3 substrates: β-catenin and the others represented by
380 MYC (**Fig. 8B**). In the presence of intact FBXW7 function, these Wnt-driven cancer cells
381 require active Wnt signaling to maintain high levels of both β-catenin and MYC. After FBXW7
382 inactivation, activation of the MYC axis no longer requires upstream Wnt/β-catenin signaling,
383 and additional cell cycle-promoting activities such as up-regulated Cyclin E emerge (**Fig. 8B**).
384 We speculate that these allow the *FBXW7*-mutant cancer cells to undergo signaling and
385 transcriptional rewiring under Wnt-low conditions that eventually makes β-catenin dispensable.
386 Notably, the high Wnt/β-catenin activity in *RNF43*-mutant/*RSPO*-fusion cancer cells relies on
387 sufficient paracrine and/or autocrine Wnt ligands that may come from the tumor

388 microenvironment and may be spatiotemporally restricted. Reliance on these exogenous Wnt
389 ligands may restrict cancer progression, e.g., from outgrowing the source of Wnts, or from
390 metastasizing to Wnt-ligand deficient environment. Under these circumstances, *FBXW7*-
391 mutant cancer cells that lost β-catenin dependence would gain a survival or proliferation
392 advantage. Last but not least, inactivation of FBXW7 was recently linked to cancer immune
393 evasion[50], which also favors the selection of *FBXW7*-mutant cancer cells during tumor
394 evolution.

395 Previously we showed in pancreatic cancer that Wnt/β-catenin signaling is important in
396 tumors with an active intrinsic differentiation program which is reflected in the high expression
397 of the pancreatic differentiation master regulator GATA6. The balance between Wnt signaling
398 and the differentiation program leads to a well/moderately differentiated malignant state[18]. In
399 pancreatic tumors whose differentiation program is intrinsically blocked, e.g., by silencing
400 *GATA6* expression, tumors are dedifferentiated and Wnt/β-catenin signaling becomes
401 dispensable[18]. In our current study, we observed similar dedifferentiation and phenotypic
402 transition in *FBXW7*-mutant *RNF43*-mutant/*RSPO*-fusion cancers originated from pancreas,
403 bile duct, and large intestine. This effect could be mediated in part by the stabilized MYC
404 protein, as MYC overexpression has been shown to induce the expression of embryonic stem
405 cell genes and cause the loss of tissue and lineage specificity due to dedifferentiation in cancers
406 derived from diverse lineages[51] (**Fig. 8B**). Moreover, several studies have shown that
407 inactivation of FBXW7 promotes epithelial-mesenchymal transition (EMT) in multiple cancer
408 types, although the underlying mechanisms appear to be diverse and involve the direct or
409 indirect up-regulation of EMT factors such as Snail, Twist, or Zeb[52–55]. As EMT is an important
410 mechanism of epithelial cell dedifferentiation, *FBXW7* mutations in *RNF43*-mutant/*RSPO*-
411 fusion cancers may promote their dedifferentiation through inducing EMT (**Fig. 8B**), which is
412 consistent with their mesenchymal features.

413 Last but not least, the *FBXW7* mutation status can serve as a biomarker to stratify *RNF43*-
414 mutant/*RSPO*-fusion cancer patients for anti-Wnt therapies. *FBXW7* mutations may cause
415 primary resistance to any therapy that targets the transcriptional activity of β-catenin. Notably,
416 around one quarter of *FBXW7* mutations are missense variants of unknown significance (VUS),
417 highlighting the importance of comprehensively characterizing these VUS. As an alternative
418 strategy, we demonstrated that these *FBXW7*-mutant tumors were sensitive to multi-CDK
419 inhibitor dinaciclib that targets both cell cycle and transcription. While treatment with
420 dinaciclib alone did not achieve complete tumor growth inhibition, developing drug

421 combinations based on dinaciclib or other multi-CDK inhibitors is a promising strategy to
422 enhance the therapeutic efficacy. And whether such dinaciclib sensitivity is related to the
423 *RNF43*-mutant/*RSPO*-fusion genetic background or it can be generalized to any *FBXW7*-
424 mutant cancers deserve further investigation.

425 Materials and methods

426 Mutation analysis

427 We reviewed the literature[4,56] and public cancer genomics databases including cBioportal[57],
428 GENIE[58], and ChimerDB4[59] to identify *PTPRK-RSPO3* fusion positive colorectal tumor cases
429 with gene mutation data available. This led to the identification of 40 non-redundant cases.
430 Gene alterations in *FBXW7*, *APC*, *AXIN1*, or *CTNNB1* were extracted from the corresponding
431 databases for these 40 samples.

432 For the *RNF43*-mutant pan-cancer analysis, 1510 *RNF43*-mutant tumor samples were
433 identified out of 69223 non-redundant tumor cases collected in the cBioportal database. 81
434 samples carrying benign missense variants in *RNF43*, according to previous characterization
435 studies, were excluded. The remaining 1429 samples were classified based on the *RNF43*
436 mutation types. Gene alterations in *FBXW7*, *APC*, *AXIN1*, or *CTNNB1* were extracted from
437 cBioportal for these 1429 samples.

438 Gene alteration information for the preclinical models used in this study was extracted from
439 the DepMap database and selected references[26,27,60,61].

440 Cell culture

441 The sources of cell lines used in this study are described in Supplementary Table S1. All
442 cell lines were cultured in the corresponding culture medium recommended by the suppliers
443 supplemented with 1% (v/v) penicillin/streptomycin (Gibco, #15140122) and in a humidified
444 incubator with 5% CO_2. All cell lines were regularly tested for mycoplasma contamination and
445 confirmed to be mycoplasma free.

446 Lentiviruses and retroviruses were produced by co-transfecting the transfer plasmids with
447 pMD2.G (Addgene #12259, a gift from Didier Trono) and psPAX2 (Addgene #12260, a gift
448 from Didier Trono) or pCL-Eco (Addgene #12371, a gift from Inder Verma)[62] into HEK293FT
449 cells, as previously described[18]. The transfer plasmids used in this study included
450 FuCas9Cherry (Addgene #70182, a gift from Marco Herold)[63] for constitutively expressing
451 Cas9 protein, Lenti-dCas9-KRAB-blast (Addgene #89567, a gift from Gary Hon)[64] for
452 constitutively expressing dCas9-KRAB fusion protein, FgH1tUTG (Addgene #70183, a gift

453 from Marco Herold)[63] for expressing doxycycline (dox) inducible sgRNA, pHR'CMV-
454 FBXW7^{R465C} (a gift from Patrick Tan)[65] for expressing the mutant FBXW7, MSCV MYC
455 T58A puro (Addgene #18773, a gift from Scott Lowe)[66] for expressing the mutant MYC, and
456 MIGR1-Cyclin E-AA (Addgene #47498, a gift from Alex Minella)[67] for expressing the mutant
457 Cyclin E. After transduction, cells were selected with the corresponding antibiotics or
458 fluorescence-activated cell sorting (FACS).

459 **Soft agar colony formation assay**

460 The assay was performed as described previously[18]. Briefly, 0.6% (g/ml) agarose (Sigma,
461 A9045) in 200 µl complete culture media was dispensed into each well of 48-well suspension
462 culture plates to form the bottom layer. After solidification of the bottom layer, 3000 cells
463 mixed with 0.36% (g/ml) agarose in 200 µl complete culture media were layered on top of that.
464 After solidification of the cell/agarose layer, 450 µl complete culture media containing DMSO
465 (0.1% v/v) or ETC-159 were added to each well. Cells were cultured for 1-2 weeks to form
466 colonies. Colonies were stained with MTT and counted by GelCount (Oxford Optronix).

467 **CRISPR genome/epigenome editing**

468 sgRNAs listed in Supplementary Table S1 were cloned into the dox-inducible sgRNA
469 expression vector FgH1tUTG following the protocol described previously[63]. To knockout
470 (truncate) FBXW7, HPAF-II cells stably expressing Cas9 protein were transduced with an
471 inducible sgRNA targeting *FBXW7* (sgFBXW7#1) or a non-targeting control (sgNTC#1).
472 Transduced cells were treated with 1 µg/ml dox for 3 days (for *in vitro* assays) or 7 days (to
473 generate cells for injection into mice) to induce the sgRNA expression and genome editing. To
474 analyze the genome editing, genomic DNA was extracted from the cell pellets using a salting
475 out protocol as described previously. PCR was performed to amplify the genomic region
476 covering the expected cutting site. The PCR amplicons were purified and subject to Sanger
477 sequencing, and the indels were visualized using TIDE[68].

478 To knockdown *CTNNB1* or *MYC*, HPAF-II, HuCCT1, or AsPC-1 cells stably expressing
479 the dCas9-KRAB fusion protein were transduced with inducible sgRNAs targeting the
480 promoters of *CTNNB1* or *MYC* or a non-targeting control. To examine the gene knockdown
481 effects, transduced cells were treated with 1 µg/ml dox *in vitro* for 4 days and subject to RNA
482 extraction and qPCR analysis. Due to the short half-life of dox at 37°C, all dox-containing
483 media were changed every two days.

484 **Animal studies**

485 Animal experiments were performed in NOD scid gamma (NSG) mice purchased from
486 InVivos, Singapore or The Jackson Laboratory and bred and housed in specific pathogen-free
487 conditions. For subcutaneous implantation, cancer cells were harvested from cell culture,
488 washed with cold PBS, and resuspended in ice cold 50% Matrigel (Corning, #354248) in PBS.
489 5×10^6 cells in 200 µl 50% Matrigel were injected into the flank of NSG mice. Tumor
490 dimensions were measured using a caliper and tumor volumes were calculated as 0.5 × length
491 × $(\text{width})^2$. For drug administration, ETC-159 was formulated in 50% (v/v) PEG400 in water
492 and administered by oral gavage at a dosing volume of 5 µl/g mouse body weight following
493 the dosing schedule indicated in each experiment. Dinaciclib was formulated in 20% (g/ml) (2-
494 hydroxypropyl)-β-cyclodextrin in water and administered by intraperitoneal injection at a
495 dosing volume of 5 µl/g mouse body weight following the dosing schedule indicated in each
496 experiment. To induce the sgRNA expression *in vivo*, mice were fed *ad libitum* with standard
497 diet containing 600 mg doxycycline/kg (Specialty Feeds, SF08-026) until the end of the study.
498 The tumors and organs with metastases, if any, were harvested and snap-frozen in liquid
499 nitrogen followed by storage at -80 °C, or immediately fixed in 10% neutral buffered formalin
500 for two days at room temperature followed by paraffin embedding. The SingHealth
501 Institutional Animal Care and Use Committee approved all animal studies, which compiled
502 with applicable regulations.

503 **Western blotting**

504 Fresh cells or snap-frozen tumor tissues were homogenized in 4% SDS in water using a
505 tissue homogenizer. Protein concentration of the lysate was measured by the bicinchoninic acid
506 (BCA) assay. Equal amounts of total protein of each sample were resolved by 10% SDS-PAGE
507 followed by wet transfer to PVDF membranes. Western blotting was performed following
508 standard methods. Primary and secondary antibodies used in this study are described in
509 Supplementary Table S1. The SuperSignal West Dura Extended Duration Substrate (Thermo
510 Scientific, #34075) or Cytiva Amersham ECL Select Western Blotting Detection Reagent
511 (Fischer Scientific, #45000999) were used for developing the chemiluminescence blots. The
512 images were captured digitally using the Bio-Rad ChemiDoc Touch Imaging system or the LI-
513 COR Odyssey Imaging system.

514 **Histological analysis**

515 Formalin-fixed paraffin-embedded tissue sections were deparaffinized and rehydrated.
516 Hematoxylin and Eosin (H&E) staining was performed with standard methods.
517 Immunohistochemistry (IHC) for β-catenin, GFP, and Ki67 was performed as described

518 previously[18]. Antibodies used for IHC are described in Supplementary Table S1. Alcian blue
519 (pH 2.5) mucin staining was performed using the Alcian Blue Stain Kit (Abcam, ab150662).
520 Bright field images were taken with a Nikon ECLIPSE Ni-E microscope.

521 **RNA extraction and quantitative PCR (qPCR)**

522 Total RNA from fresh cells or snap-frozen tumor tissues was extracted using the QIAGEN
523 RNeasy Kit. cDNA was synthesized using the MiRXES BlitzAmp cDNA synthesis kit. Real
524 time qPCR was performed using the Bio-Rad SsoAdvanced Universal SYBR Green Supermix
525 on Bio-Rad CFX96 or CFX384 Touch real-time PCR machines. Primer sequences are
526 described in Supplementary Table S1. All qPCR primers are human specific.

527 **Gene set enrichment analysis (GSEA)**

528 Transcriptomic data of the *RSPO3*-fusion colorectal PDXs treated with RSPO3-
529 neutralizing antibody or control were extracted from GSE73906[15]. Gene set enrichment
530 analysis was performed using the GSEA software (www.gsea-msigdb.org)[69].

531 **Statistical analysis**

532 Statistical analyses were performed using GraphPad Prism 10 or as otherwise stated. Two-
533 tailed unpaired *t* tests were used to analyze data involving direct comparison between an
534 experimental group and a control group. P value < 0.05 or FDR < 0.1 were considered to be
535 statistically significant.

536 Author contributions

537 ZZ and DMV designed the study. ZZ performed the experiments and analyses. DMV
538 supervised the study. ZZ and DMV wrote the manuscript.

539 Acknowledgements

540 We gratefully acknowledge Yunka Wong and Xinang Cao for their invaluable technical
541 supports and advice. We thank members of the Virshup lab for useful discussions. This
542 research was supported in part by the National Research Foundation Singapore and
543 administered by the Ministry of Health's National Medical Research Council under Singapore
544 Translational Research (STaR) Award MOH-000155 (to DMV). Figure 5A was created with
545 BioRender.com.

546 ## References

547 1. Zhong, Z. & Virshup, D. M. Wnt Signaling and Drug Resistance in Cancer. *Mol.*
548 *Pharmacol.* **97**, 72–89 (2020).

549 2. Zhong, Z., Yu, J., Virshup, D. M. & Madan, B. Wnts and the hallmarks of cancer. *Cancer*
550 *Metastasis Rev.* **39**, 625–645 (2020).

551 3. Jiang, X. *et al.* Inactivating mutations of RNF43 confer Wnt dependency in pancreatic
552 ductal adenocarcinoma. *PNAS* **110**, 12649–12654 (2013).

553 4. Seshagiri, S. *et al.* Recurrent R-spondin fusions in colon cancer. *Nature* **488**, 660–664
554 (2012).

555 5. Waddell, N. *et al.* Whole genomes redefine the mutational landscape of pancreatic cancer.
556 *Nature* **518**, 495–501 (2015).

557 6. Bailey, P. *et al.* Genomic analyses identify molecular subtypes of pancreatic cancer.
558 *Nature* **531**, 47–52 (2016).

559 7. Network, C. G. A. R. Integrated Genomic Characterization of Pancreatic Ductal
560 Adenocarcinoma. *Cancer Cell* **32**, 185-203.e13 (2017).

561 8. Seeber, A. *et al.* Comprehensive analysis of R-spondin fusions and RNF43 mutations
562 implicate novel therapeutic options in colorectal cancer. *Clin. Cancer Res.* (2022)
563 doi:10.1158/1078-0432.ccr-21-3018.

564 9. Hashimoto, T. *et al.* Clinicopathological and molecular characteristics of RSPO fusion-
565 positive colorectal cancer. *Brit J Cancer* 1–8 (2022) doi:10.1038/s41416-022-01880-w.

566 10. Madan, B. *et al.* Wnt addiction of genetically defined cancers reversed by PORCN
567 inhibition. *Oncogene* **35**, 2197–2207 (2016).

568 11. Storm, E. E. *et al.* Targeting PTPRK-RSPO3 colon tumours promotes differentiation and
569 loss of stem-cell function. *Nature* **529**, 97–100 (2016).

570 12. Gurney, A. *et al.* Wnt pathway inhibition via the targeting of Frizzled receptors results in
571 decreased growth and tumorigenicity of human tumors. *PNAS* **109**, 11717–11722 (2012).

572 13. Fischer, M. M. *et al.* WNT antagonists exhibit unique combinatorial antitumor activity
573 with taxanes by potentiating mitotic cell death. *Sci Adv* **3**, e1700090 (2017).

574 14. Steinhart, Z. *et al.* Genome-wide CRISPR screens reveal a Wnt-FZD5 signaling circuit as
575 a druggable vulnerability of RNF43-mutant pancreatic tumors. *Nat. Med.* **23**, 60–68 (2017).

576 15. Chartier, C. *et al.* Therapeutic Targeting of Tumor-Derived R-Spondin Attenuates β-
577 Catenin Signaling and Tumorigenesis in Multiple Cancer Types. *Cancer Res.* **76**, 713–723
578 (2016).

579 16. Rodon, J. *et al.* Phase 1 study of single-agent WNT974, a first-in-class Porcupine
580 inhibitor, in patients with advanced solid tumours. *Br J Cancer* (2021) doi:10.1038/s41416-
581 021-01389-8.

582 17. Giannakis, M. *et al.* Phase 1 study of WNT pathway Porcupine inhibitor CGX1321 and
583 phase 1b study of CGX1321 + pembrolizumab (pembro) in patients (pts) with advanced
584 gastrointestinal (GI) tumors. *J. Clin. Oncol.* **41**, 3514–3514 (2023).

585 18. Zhong, Z., Harmston, N., Wood, K. C., Madan, B. & Virshup, D. M. A p300/GATA6
586 axis determines differentiation and Wnt dependency in pancreatic cancer models. *J Clin*
587 *Investigation* **132**, e156305 (2022).

588 19. O'Brien, S. *et al.* SCFFBXW7 regulates G2-M progression through control of CCNL1
589 ubiquitination. *Embo Rep* e55044 (2022) doi:10.15252/embr.202255044.

590 20. Davis, R. J., Welcker, M. & Clurman, B. E. Tumor suppression by the Fbw7 ubiquitin
591 ligase: mechanisms and opportunities. *Cancer Cell* **26**, 455–464 (2014).

592 21. Tu, J. *et al.* The most common RNF43 mutant G659Vfs*41 is fully functional in
593 inhibiting Wnt signaling and unlikely to play a role in tumorigenesis. *Sci Rep* **9**, 18557
594 (2019).

595 22. Li, S. *et al.* Commonly observed RNF43 mutations retain functionality in attenuating
596 Wnt/β-catenin signaling and unlikely confer Wnt-dependency onto colorectal cancers.
597 *Oncogene* **485**, 195–15 (2020).

598 23. Yu, J. *et al.* The functional landscape of patient-derived RNF43 mutations predicts
599 sensitivity to Wnt inhibiton. *Cancer Res.* canres.0957.2020 (2020) doi:10.1158/0008-
600 5472.can-20-0957.

601 24. Yan, H. H. N. *et al.* RNF43 germline and somatic mutation in serrated neoplasia pathway
602 and its association with BRAF mutation. *Gut* **66**, 1645–1656 (2017).

603 25. Elez, E. *et al.* RNF43 mutations predict response to anti-BRAF/EGFR combinatory
604 therapies in BRAFV600E metastatic colorectal cancer. *Nat Med* 1–9 (2022)
605 doi:10.1038/s41591-022-01976-z.

606 26. Zhong, Z. *et al.* PORCN inhibition synergizes with PI3K/mTOR inhibition in Wnt-
607 addicted cancers. *Oncogene* **38**, 6662–6677 (2019).

608 27. Picco, G. *et al.* Loss of AXIN1 drives acquired resistance to WNT pathway blockade in
609 colorectal cancer cells carrying RSPO3 fusions. *EMBO Molecular Medicine* **9**, 293–303
610 (2017).

611 28. Madan, B. *et al.* Temporal dynamics of Wnt-dependent transcriptome reveal an
612 oncogenic Wnt/MYC/ribosome axis. *J. Clin. Invest.* **128**, 5620–5633 (2018).

613 29. Zhang, L. *et al.* Integrated stability and activity control of the Drosophila Rbf1
614 retinoblastoma protein. *J. Biol. Chem.* **289**, 24863–24873 (2014).

615 30. Wang, Y. *et al.* A Novel Retinoblastoma Protein (RB) E3 Ubiquitin Ligase (NRBE3)
616 Promotes RB Degradation and Is Transcriptionally Regulated by E2F1 Transcription Factor*.
617 *J. Biol. Chem.* **290**, 28200–28213 (2015).

618 31. Wang, C. *et al.* Myeloid FBW7 deficiency disrupts redox homeostasis and aggravates
619 dietary-induced insulin resistance. *Redox Biol* **37**, 101688 (2020).

620 32. Hart, M. *et al.* The F-box protein beta-TrCP associates with phosphorylated beta-catenin
621 and regulates its activity in the cell. *Curr. Biol.* **9**, 207–210 (1999).

622 33. Collisson, E. A. *et al.* Subtypes of pancreatic ductal adenocarcinoma and their differing
623 responses to therapy. *Nat. Med.* **17**, 500–503 (2011).

624 34. Moffitt, R. A. *et al.* Virtual microdissection identifies distinct tumor- and stroma-specific
625 subtypes of pancreatic ductal adenocarcinoma. *Nat. Genet.* **47**, 1168–1178 (2015).

626 35. Hayashi, A. *et al.* A unifying paradigm for transcriptional heterogeneity and squamous
627 features in pancreatic ductal adenocarcinoma. *Nat Cancer* **1**, 59–74 (2020).

628 36. Vasquez, E. G. *et al.* Dynamic and adaptive cancer stem cell population admixture in
629 colorectal neoplasia. *Cell Stem Cell* **29**, 1213-1228.e8 (2022).

630 37. Leach, J. D. G. *et al.* Oncogenic BRAF, unrestrained by TGFβ-receptor signalling, drives
631 right-sided colonic tumorigenesis. *Nat Commun* **12**, 3464 (2021).

632 38. Guinney, J. *et al.* The consensus molecular subtypes of colorectal cancer. *Nat. Med.* **21**,
633 1350–1356 (2015).

634 39. Nie, Z. *et al.* c-Myc Is a Universal Amplifier of Expressed Genes in Lymphocytes and
635 Embryonic Stem Cells. *Cell* **151**, 68–79 (2012).

636 40. Lin, C. Y. *et al.* Transcriptional Amplification in Tumor Cells with Elevated c-Myc. *Cell*
637 **151**, 56–67 (2012).

638 41. Chou, J., Quigley, D. A., Robinson, T. M., Feng, F. Y. & Ashworth, A. Transcription-
639 Associated Cyclin-Dependent Kinases as Targets and Biomarkers for Cancer Therapy.
640 *Cancer Discov.* **10**, 351–370 (2020).

641 42. Parry, D. *et al.* Dinaciclib (SCH 727965), a novel and potent cyclin-dependent kinase
642 inhibitor. *Mol. Cancer Ther.* **9**, 2344–2353 (2010).

643 43. Johnson, S. F. *et al.* CDK12 Inhibition Reverses De Novo and Acquired PARP Inhibitor
644 Resistance in BRCA Wild-Type and Mutated Models of Triple-Negative Breast Cancer. *Cell*
645 *Rep* **17**, 2367–2381 (2016).

646 44. Freeman-Cook, K. *et al.* Expanding control of the tumor cell cycle with a CDK2/4/6
647 inhibitor. *Cancer Cell* **39**, 1404-1421.e11 (2021).

648 45. Scaltriti, M. *et al.* Cyclin E amplification/overexpression is a mechanism of trastuzumab
649 resistance in HER2+ breast cancer patients. *PNAS* **108**, 3761–3766 (2011).

650 46. Wander, S. A. *et al.* The Genomic Landscape of Intrinsic and Acquired Resistance to
651 Cyclin-Dependent Kinase 4/6 Inhibitors in Patients with Hormone Receptor–Positive
652 Metastatic Breast Cancer. *Cancer Discov.* **10**, 1174–1193 (2020).

653 47. Rihawi, K. *et al.* MYC Amplification as a Potential Mechanism of Primary Resistance to
654 Crizotinib in ALK-Rearranged Non-Small Cell Lung Cancer: A Brief Report. *Transl. Oncol.*
655 **12**, 116–121 (2019).

656 48. Iyer, S. R. *et al.* MYC promotes tyrosine kinase inhibitor resistance in ROS1 fusion-
657 positive lung cancer. *Mol. Cancer Res.* **20**, molcanres.MCR-22-0025-E.2022 (2022).

658 49. Lin, J. J. *et al.* Spectrum of Mechanisms of Resistance to Crizotinib and Lorlatinib in
659 ROS1 Fusion–Positive Lung Cancer. *Clin. Cancer Res.* **27**, 2899–2909 (2021).

660 50. Gstalder, C. *et al.* Inactivation of Fbxw7 impairs dsRNA sensing and confers resistance to
661 PD-1 blockade. *Cancer Discovery* CD-19-1416 (2020) doi:10.1158/2159-8290.cd-19-1416.

662 51. Sullivan, D. K. *et al.* MYC oncogene elicits tumorigenesis associated with embryonic,
663 ribosomal biogenesis, and tissue-lineage dedifferentiation gene expression changes.
664 *Oncogene* **41**, 4960–4970 (2022).

665 52. Cuevas, I. C. *et al.* Fbxw7 is a driver of uterine carcinosarcoma by promoting epithelial-
666 mesenchymal transition. *Proc. Natl. Acad. Sci. United States Am.* **116**, 25880–25890 (2019).

667 53. Zhang, Y. *et al.* FBW7 loss promotes epithelial-to-mesenchymal transition in non-small
668 cell lung cancer through the stabilization of Snail protein. *Cancer Lett.* **419**, 75–83 (2018).

669 54. Yang, H. *et al.* FBXW7 suppresses epithelial-mesenchymal transition, stemness and
670 metastatic potential of cholangiocarcinoma cells. *Oncotarget* **6**, 6310–6325 (2015).

671 55. Li, N. *et al.* An FBXW7-ZEB2 axis links EMT and tumour microenvironment to promote
672 colorectal cancer stem cells and chemoresistance. *Oncogenesis* **8**, 13 (2019).

673 56. Singh, H. *et al.* Molecular Characterization and Therapeutic Targeting of Colorectal
674 Cancers Harboring Receptor Tyrosine Kinase Fusions. *Clin. Cancer Res.* **27**, 1695–1705
675 (2021).

676 57. Cerami, E. *et al.* The cBio Cancer Genomics Portal: An Open Platform for Exploring
677 Multidimensional Cancer Genomics Data. *Cancer Discov.* **2**, 401–404 (2012).

678 58. Consortium, T. A. P. G. *et al.* AACR Project GENIE: Powering Precision Medicine
679 through an International Consortium. *Cancer Discov.* **7**, 818–831 (2017).

680 59. Jang, Y. E. *et al.* ChimerDB 4.0: an updated and expanded database of fusion genes.
681 *Nucleic Acids Res.* **48**, D817–D824 (2020).

682 60. Rospo, G. *et al.* Evolving neoantigen profiles in colorectal cancers with DNA repair
683 defects. *Genome Med* **11**, 42 (2019).

684 61. Zhang, C. *et al.* Abstract 404: Development of a RSPO3 CLIA-validated assay as a
685 predictive biomarker for response to anti-RSPO3 antibody treatment in patients with solid
686 tumors. *Cancer Res.* **76**, 404–404 (2016).

687 62. Naviaux, R. K., Costanzi, E., Haas, M. & Verma, I. M. The pCL vector system: rapid
688 production of helper-free, high-titer, recombinant retroviruses. *J. Virol.* **70**, 5701–5 (1996).

689 63. Aubrey, B. J. *et al.* An inducible lentiviral guide RNA platform enables the identification
690 of tumor-essential genes and tumor-promoting mutations in vivo. *Cell Rep* **10**, 1422–1432
691 (2015).

692 64. Xie, S., Duan, J., Li, B., Zhou, P. & Hon, G. C. Multiplexed Engineering and Analysis of
693 Combinatorial Enhancer Activity in Single Cells. *Mol. Cell* **66**, 285-299.e5 (2017).

694 65. Huang, K. K. *et al.* Genomic and Epigenomic Profiling of High-Risk Intestinal
695 Metaplasia Reveals Molecular Determinants of Progression to Gastric Cancer. *Cancer Cell*
696 **33**, 137-150.e5 (2018).

697 66. Hemann, M. T. *et al.* Evasion of the p53 tumour surveillance network by tumour-derived
698 MYC mutants. *Nature* **436**, 807–811 (2005).

699 67. Xu, Y., Swartz, K. L., Siu, K. T., Bhattacharyya, M. & Minella, A. C. Fbw7-dependent
700 cyclin E regulation ensures terminal maturation of bone marrow erythroid cells by restraining
701 oxidative metabolism. *Oncogene* **33**, 3161–3171 (2014).

702 68. Brinkman, E. K., Chen, T., Amendola, M. & Steensel, B. van. Easy quantitative
703 assessment of genome editing by sequence trace decomposition. *Nucleic Acids Res.* **42**, e168
704 (2014).

705 69. Subramanian, A. *et al.* Gene set enrichment analysis: A knowledge-based approach for
706 interpreting genome-wide expression profiles. *Proc. Natl. Acad. Sci.* **102**, 15545–15550
707 (2005).

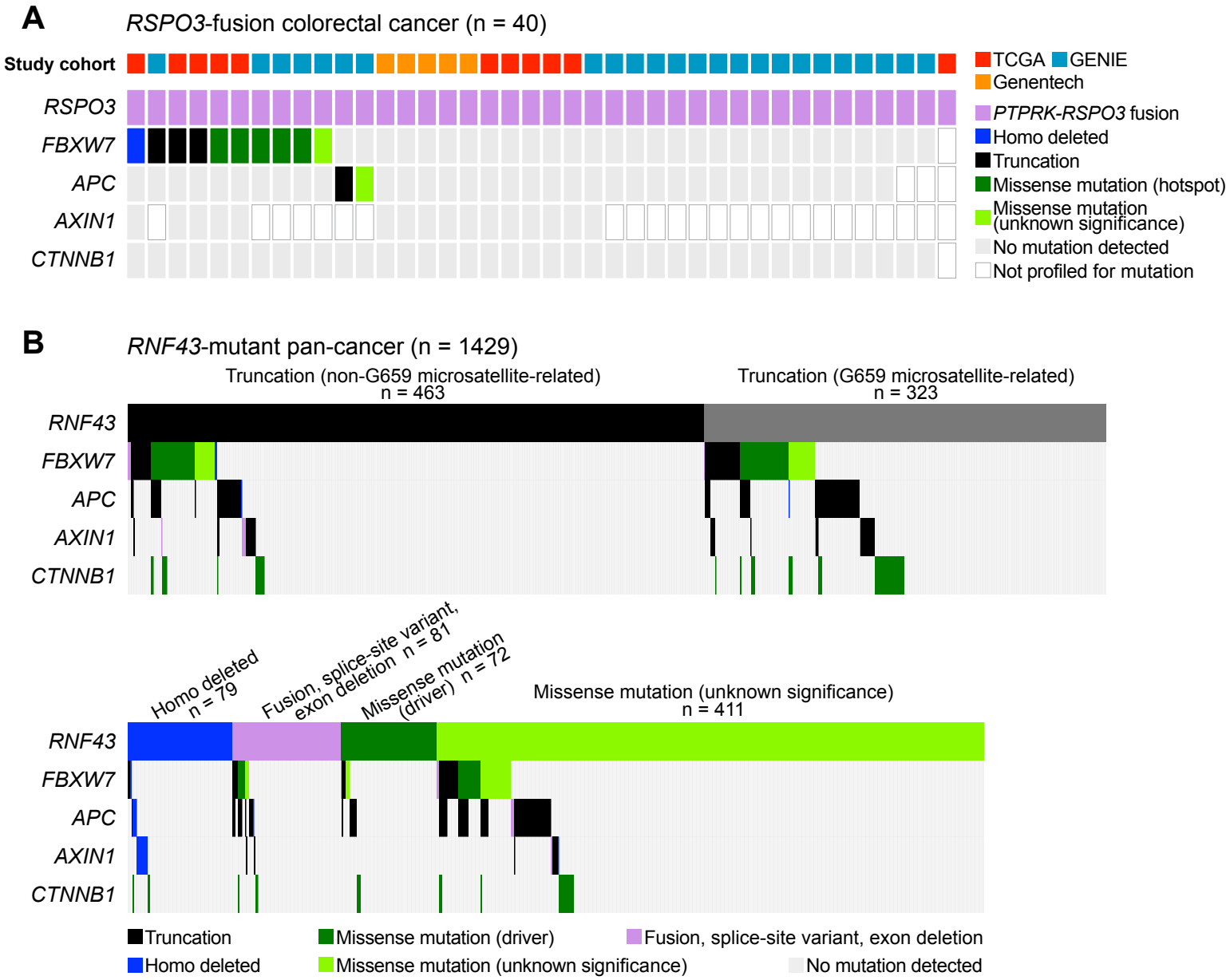
A
RSPO3-fusion colorectal cancer (n = 40)
Study cohort
RSPO3
FBXW7
APC
AXIN1
CTNNB1
TCGA
GENIE
Genentech
PTPRK-RSPO3 fusion
Homo deleted
Truncation
Missense mutation (hotspot)
Missense mutation (unknown significance)
No mutation detected
Not profiled for mutation
B
RNF43-mutant pan-cancer (n = 1429)
Truncation (non-G659 microsatellite-related) n = 463
Truncation (G659 microsatellite-related) n = 323
RNF43
FBXW7
APC
AXIN1
CTNNB1
Homo deleted n = 79
Fusion, splice-site variant, exon deletion n = 81
Missense mutation (driver) n = 72
Missense mutation (unknown significance) n = 411
Truncation
Missense mutation (driver)
Fusion, splice-site variant, exon deletion
Homo deleted
Missense mutation (unknown significance)
No mutation detected

Figure 1

Figure 1. Recurrent *FBXW7* mutations in *RNF43*-mutant/*RSPO*-fusion cancers.

(A) Recurrent *FBXW7* mutations in 10 (25%) individuals in a combined cohort of 40 *PTPRK-RSPO3* fusion colorectal tumors. Each column represents an individual tumor sample.

(B) Mutations in *FBXW7*, *APC*, *AXIN1*, and *CTNNB1* in 1429 *RNF43*-mutant tumors regardless of tumor origin (pan-cancer). Each column represents an individual tumor sample, grouped based on the type of *RNF43* mutations. For *APC*, *AXIN1*, and *CTNNB1*, only established Wnt/β-catenin-activating mutations such as *APC*/*AXIN1* truncation/deletion and hotspot *CTNNB1* stabilizing mutations are shown, while missense mutations that are empirically recognized as probable wildtype-like passenger mutations are not shown.

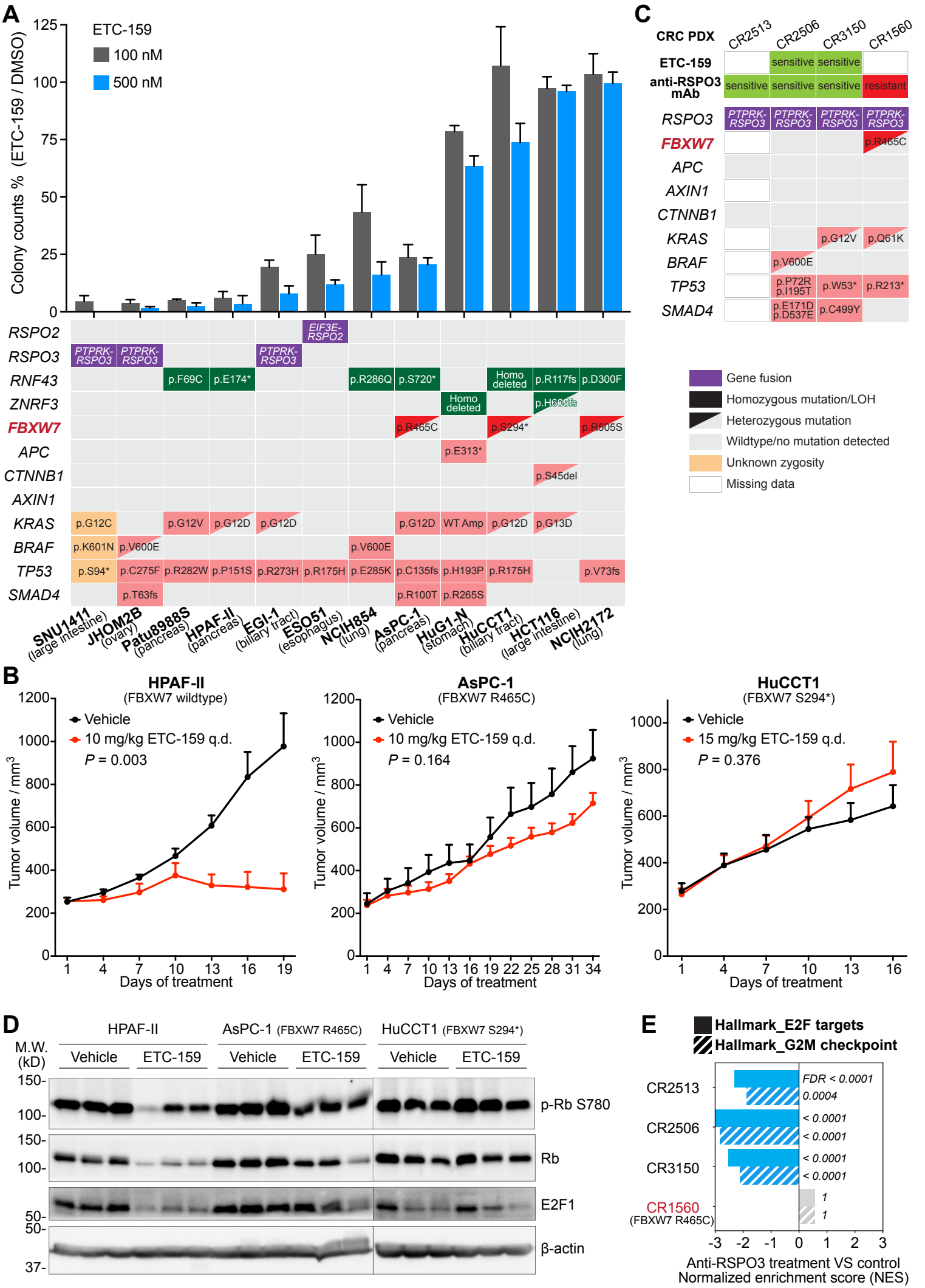
A
ETC-159
100 nM
500 nM
Colony counts % (ETC-159 / DMSO)
RSPO2
RSPO3
RNF43
ZNRF3
FBXW7
APC
CTNNB1
AXIN1
KRAS
BRAF
TP53
SMAD4
SNU1411 (large intestine)
JHOM2B (ovary)
Patu8988S (pancreas)
HPAF-II (pancreas)
EGI-1 (biliary tract)
ESO51 (esophagus)
NCIH854 (lung)
AsPC-1 (pancreas)
HuG1-N (stomach)
HuCCT1 (biliary tract)
HCT116 (large intestine)
NCIH2172 (lung)
B
HPAF-II (FBXW7 wildtype)
Vehicle
10 mg/kg ETC-159 q.d.
P = 0.003
AsPC-1 (FBXW7 R465C)
P = 0.164
HuCCT1 (FBXW7 S294*)
15 mg/kg ETC-159 q.d.
P = 0.376
Tumor volume / mm3
Days of treatment
C
CRC PDX
CR2513
CR2506
CR3150
CR1560
ETC-159
anti-RSPO3 mAb
Gene fusion
Homozygous mutation/LOH
Heterozygous mutation
Wildtype/no mutation detected
Unknown zygosity
Missing data
D
HPAF-II
AsPC-1 (FBXW7 R465C)
HuCCT1 (FBXW7 S294*)
Vehicle
ETC-159
M.W. (kD)
p-Rb S780
Rb
E2F1
β-actin
E
Hallmark_E2F targets
Hallmark_G2M checkpoint
CR2513
CR2506
CR3150
CR1560 (FBXW7 R465C)
FDR < 0.0001
0.0004
< 0.0001
Anti-RSPO3 treatment VS control
Normalized enrichment score (NES)

Figure 2

Figure 2. *FBXW7* mutation status predicts resistance to Wnt inhibition in *RNF43*-mutant/*RSPO*-fusion cancers.

(A) *RNF43*-mutant/*RSPO*-fusion cancer cell lines harboring inactivating mutations in *FBXW7* were resistant to PORCN inhibitor in *in vitro* colony formation assays. Cancer cells seeded in soft agar were treated with 100 or 500 nM PORCN inhibitor ETC-159 or DMSO (0.1% v/v) for 1-2 weeks. JHOM2B and HuCCT1 cells did not grow in soft agar and were examined in a low-density 2D culture assay. Colonies were quantified and data are plotted as mean + SD reflecting the relative colony formation (ETC-159-treated versus DMSO control). n = 2-4 biological replicates per condition. Genetic alterations in drug sensitizing genes (*RNF43*, *ZNRF3*, and *RSPO2*/*3*), drug resistance genes (*FBXW7*, *APC*, *AXIN1*, and *CTNNB1*), and additional oncogenic drivers are shown in the lower panel.

(B) *RNF43*/*FBXW7*-double mutant tumors were resistant to PORCN inhibitor *in vivo*. HPAF-II and AsPC-1 pancreatic cancer cells and HuCCT1 cholangiocarcinoma cells were subcutaneously injected into NSG mice. After tumor establishment, tumor-bearing mice were treated with vehicle or 10 or 15 mg/kg ETC-159 once every day (q.d.). Data are represented as mean + SEM (n = 6-8 tumors/arm). *P* values of 2-tailed, unpaired *t* test between vehicle and ETC-159 arms at the last time point are shown.

(C) An *RSPO3*-fusion colorectal cancer PDX resistant to RSPO3-neutralizing antibody harbors *FBXW7* hotspot mutation. Sensitivity of these *RSPO3*-fusion colorectal cancer PDXs to ETC-159 and the anti-RSPO3 monoclonal antibody (mAb) was reported in ref. 15.

(D, E) Wnt inhibition failed to induce cytostasis in *RNF43*-mutant/*RSPO*-fusion tumors harboring *FBXW7* mutations. **(D)** Tumors harvested from **(B)** were analysed by western blotting for cell cycle-related proteins. Each lane represents an independent tumor. **(E)** Gene set enrichment analysis (GSEA) of cell cycle-related hallmark gene sets for *RSPO3*-fusion PDXs mentioned in **(C)** treated with the RSPO3-neutralizing mAb versus control (ref. 15). The transcriptomic data were extracted from GSE73906.

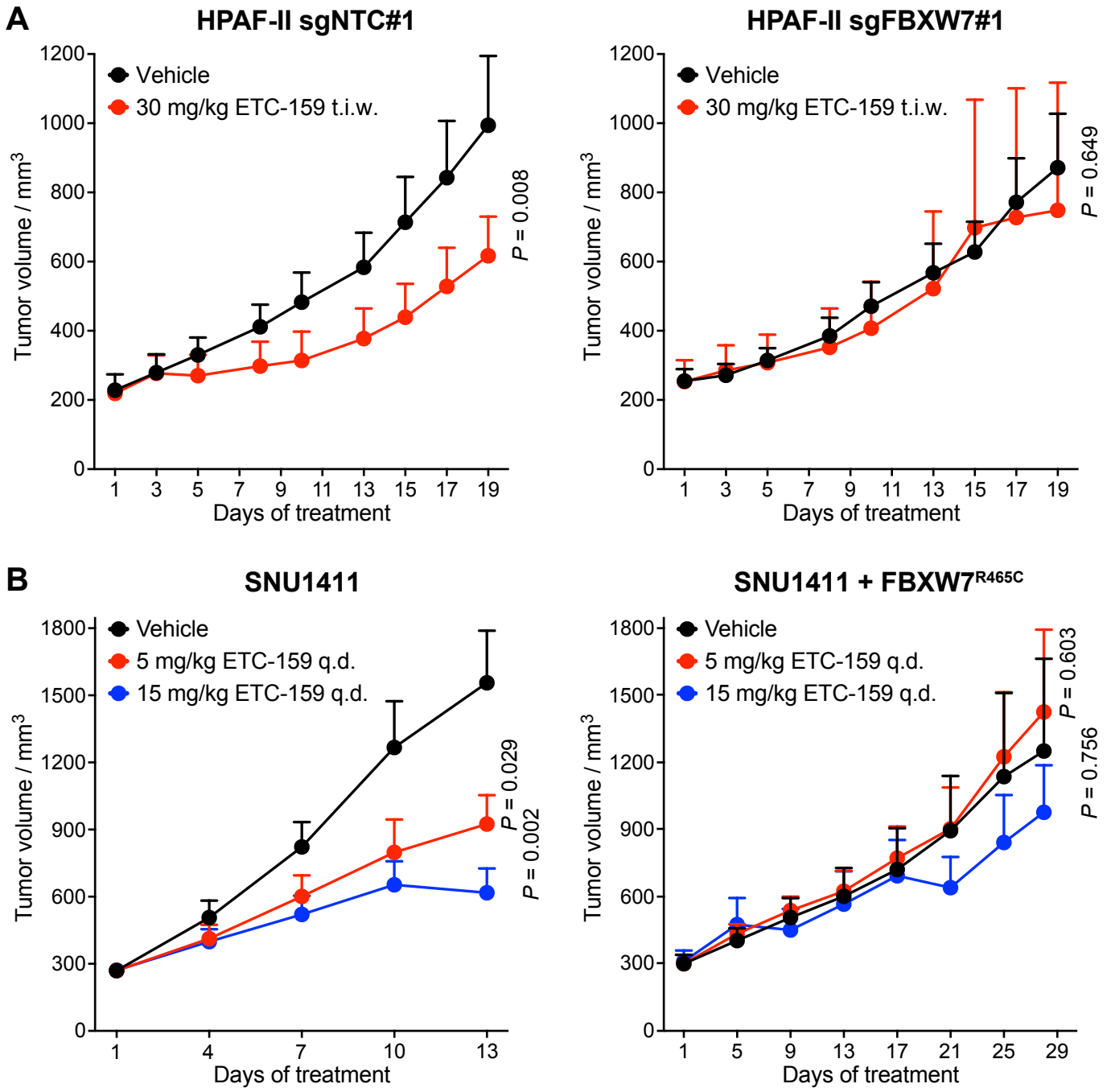
A
HPAF-II sgNTC#1
Vehicle
30 mg/kg ETC-159 t.i.w.
Tumor volume / mm3
Days of treatment
P = 0.008
HPAF-II sgFBXW7#1
Vehicle
30 mg/kg ETC-159 t.i.w.
Tumor volume / mm3
Days of treatment
P = 0.649
B
SNU1411
Vehicle
5 mg/kg ETC-159 q.d.
15 mg/kg ETC-159 q.d.
Tumor volume / mm3
Days of treatment
P = 0.029
P = 0.002
SNU1411 + FBXW7R465C
Vehicle
5 mg/kg ETC-159 q.d.
15 mg/kg ETC-159 q.d.
Tumor volume / mm3
Days of treatment
P = 0.603
P = 0.756

Figure 3

Figure 3. Inactivation of FBXW7 confers intrinsic resistance to Wnt inhibition in *RNF43*-mutant/*RSPO*-fusion cancers.

(A) Truncating the endogenous FBXW7 in *RNF43*-mutant HPAF-II tumors caused resistance to ETC-159. HPAF-II cells transduced with a non-targeting control sgRNA (sgNTC#1) or a sgRNA targeting *FBXW7* (sgFBXW7#1) were subcutaneously injected into NSG mice. After tumor establishment, tumor-bearing mice were treated with vehicle or 30 mg/kg ETC-159 three times a week (t.i.w). Data are represented as mean + SEM (n = 6-7 tumors/arm).

(B) Ectopic expression of FBXW7 p.R465C mutant (a hotspot dominant-negative mutation) in *RSPO3*-fusion SNU1411 tumors caused resistance to PORCN inhibition. SNU1411 cells or cells stably expressing the FBXW7 mutant were subcutaneously injected into NSG mice. After tumor establishment, mice were treated with vehicle or 5 or 15 mg/kg ETC-159 once every day (q.d.). Data are represented as mean + SEM (n = 6-10 tumors/arm). *P* values of 2-tailed, unpaired *t* test between vehicle and ETC-159 arms at the last time point are shown.

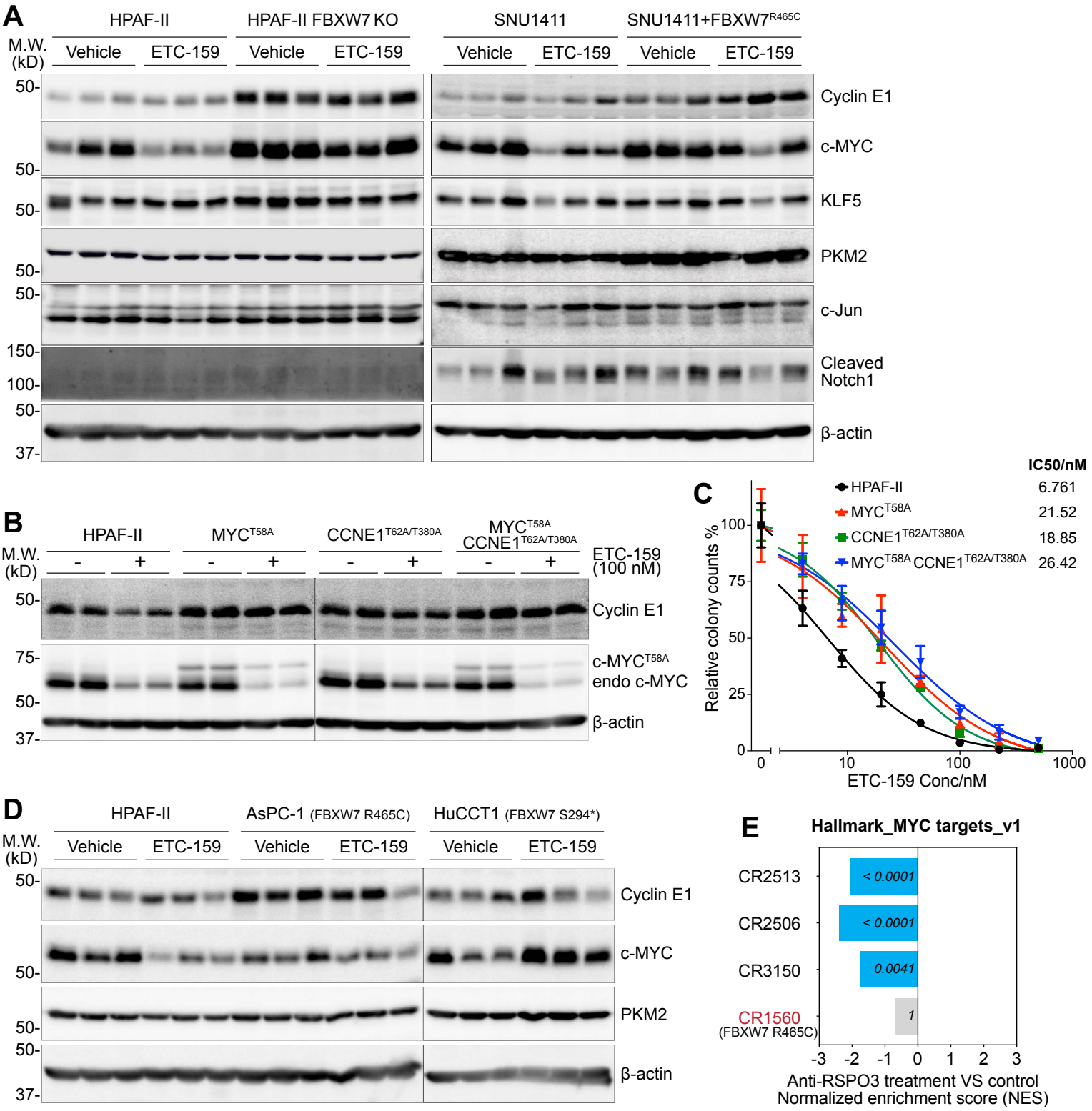
A
HPAF-II
HPAF-II FBXW7 KO
SNU1411
SNU1411+FBXW7R465C
M.W. (kD)
Vehicle
ETC-159
Cyclin E1
c-MYC
KLF5
PKM2
c-Jun
Cleaved Notch1
β-actin
B
HPAF-II
MYCT58A
CCNE1T62A/T380A
MYCT58A CCNE1T62A/T380A
ETC-159 (100 nM)
c-MYCT58A
endo c-MYC
C
IC50/nM
HPAF-II 6.761
MYCT58A 21.52
CCNE1T62A/T380A 18.85
MYCT58A CCNE1T62A/T380A 26.42
Relative colony counts %
ETC-159 Conc/nM
D
AsPC-1 (FBXW7 R465C)
HuCCT1 (FBXW7 S294*)
E
Hallmark_MYC targets_v1
CR2513
CR2506
CR3150
CR1560 (FBXW7 R465C)
< 0.0001
0.0041
1
Anti-RSPO3 treatment VS control
Normalized enrichment score (NES)

Figure 4

Figure 4. Stabilization of MYC and Cyclin E after FBXW7 inactivation causes resistance to Wnt inhibition.

(A) *RNF43*-mutant/*RSPO*-fusion cancer xenografts **(Fig. 3)** were analysed by western blotting for 6 reported substrates of FBXW7. β-actin was used as loading control. Each lane represents an independent tumor. In the panel of SNU1411 ± FBXW7 mutant, ETC-159-treated samples were from the 5 mg/kg group shown in **Fig. 3B**.

(B, C) Ectopic expression of human phosphorylation site mutant Cyclin E1 (CCNE1) or MYC that are resistant to GSK3/FBXW7-mediated degradation caused resistance to PORCN inhibition in HPAF-II cells. **(B)** HPAF-II cells or cells stably expressing the mutants were treated with DMSO or 100 nM ETC-159 for 4 days, followed by western blotting analysis. The exogenous MYC mutant was fused with 3xHA tag that led to the mobility shift on the gel. endo, endogenous. n = 2 biological replicates/condition. **(C)** HPAF-II cells or cells stably expressing the mutants were seeded in soft agar and treated with the indicated concentrations of ETC-159 for ~2 weeks. Colony numbers were quantified and normalized to the DMSO control. Data are represented as mean ± SD (n = 3 biological replicates/condition). IC50 values are shown.

(D) *RNF43*-mutant tumors with or without pre-existing *FBXW7* mutations and treated with vehicle or ETC-159 **(Fig. 2B)** were analysed by western blotting. Each lane represents an independent tumor.

(E) GSEA of the hallmark "MYC targets" gene set for *RSPO3*-fusion PDXs **(Fig. 2C)** treated with the RSPO3-neutralizing mAb versus control. The transcriptomic data were extracted from GSE73906.

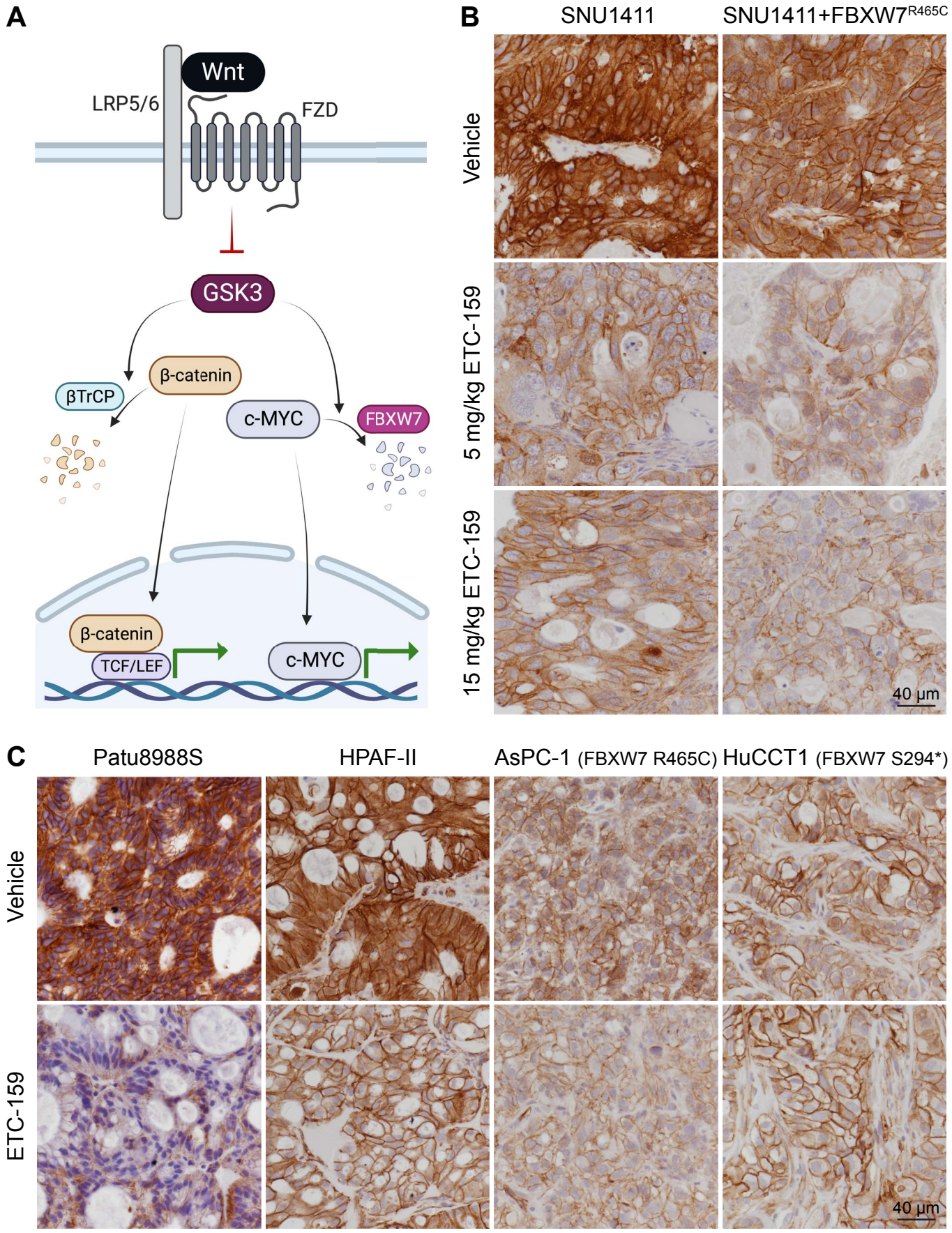
A
Wnt
LRP5/6
FZD
GSK3
β-catenin
βTrCP
c-MYC
FBXW7
β-catenin
TCF/LEF
c-MYC
B
SNU1411
SNU1411+FBXW7R465C
Vehicle
5 mg/kg ETC-159
15 mg/kg ETC-159
40 μm
C
Patu8988S
HPAF-II
AsPC-1 (FBXW7 R465C)
HuCCT1 (FBXW7 S294*)
Vehicle
ETC-159
40 μm

Figure 5

Figure 5. Inactivation of FBXW7 does not mitigate β-catenin degradation upon Wnt inhibition and *FBXW7*-mutant *RNF43*-mutant/*RSPO*-fusion cancers show low basal levels of β-catenin.

(A) Schematic model of the Wnt/GSK3-regulated β-catenin and MYC turnover. Please refer to the text for detailed description.

(B) PORCN inhibition decreased β-catenin abundance in *RSPO3*-fusion SNU1411 tumors regardless of FBXW7 status. β-catenin staining was performed on SNU1411 tumor samples with or without expressing the dominant-negative FBXW7 mutant and treated with vehicle or ETC-159 **(Fig. 3B)**.

(C) Pre-existing *RNF43*/*FBXW7*-double mutant cancer xenografts showed low basal levels of β-catenin in both cytoplasm and nucleus. β-catenin staining was performed on tumor samples harvested from experiments shown in **Fig. 2B** and our previous study (for the *RNF43*-mutant *FBXW7*-wildtype Patu8988S pancreatic cancer xenografts, ref. 18). Note that the β-catenin staining on HPAF-II, AsPC-1, and HuCCT1 samples was performed in the same batch while Patu8988S samples were assayed in another batch.

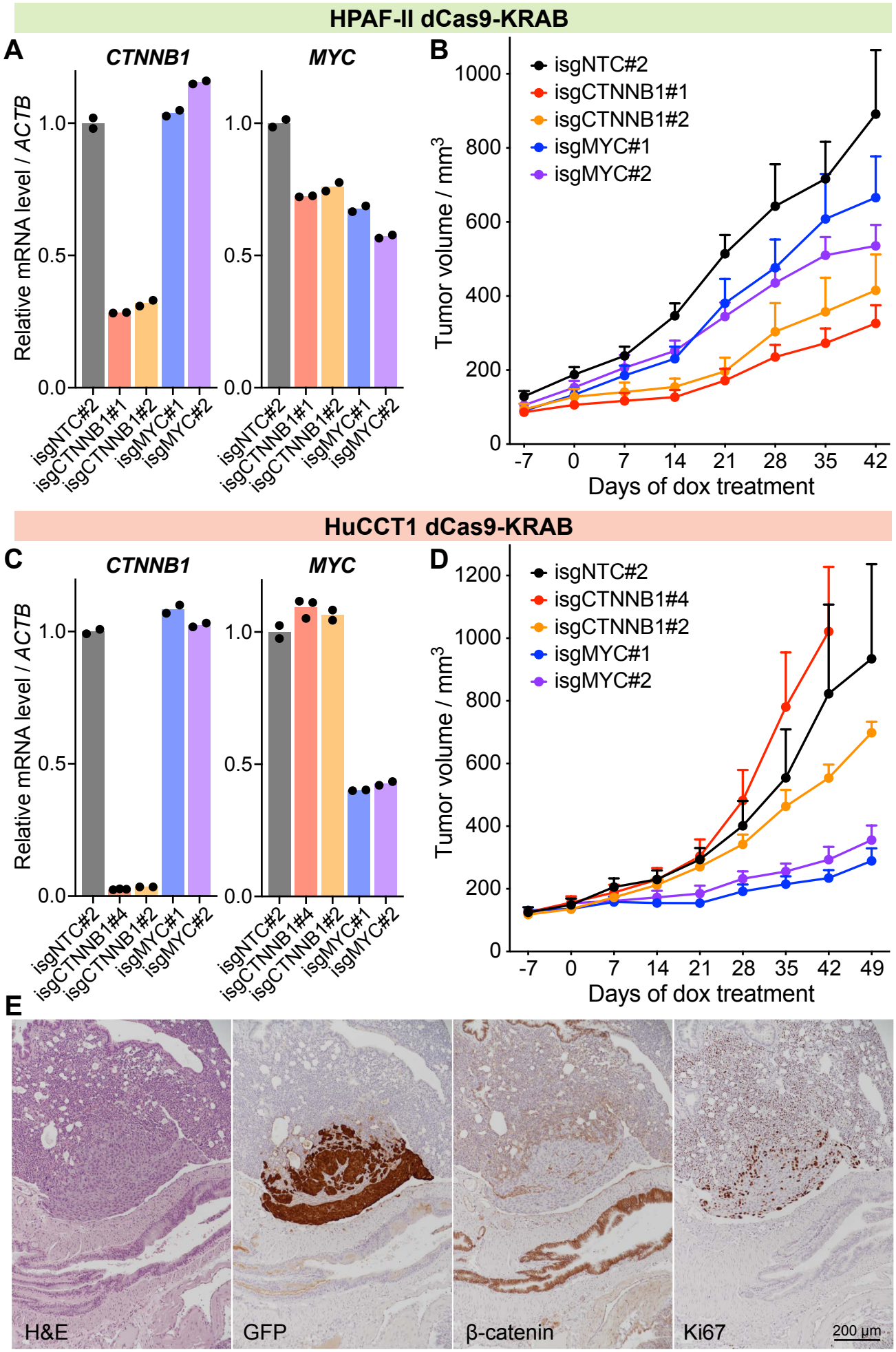
HPAF-II dCas9-KRAB
A
CTNNB1
MYC
Relative mRNA level / ACTB
1.0
0.5
0.0
isgNTC#2
isgCTNNB1#1
isgCTNNB1#2
isgMYC#1
isgMYC#2
B
isgNTC#2
isgCTNNB1#1
isgCTNNB1#2
isgMYC#1
isgMYC#2
Tumor volume / mm3
1000
800
600
400
200
0
-7
0
7
14
21
28
35
42
Days of dox treatment
HuCCT1 dCas9-KRAB
C
CTNNB1
MYC
Relative mRNA level / ACTB
isgNTC#2
isgCTNNB1#4
isgCTNNB1#2
isgMYC#1
isgMYC#2
D
isgNTC#2
isgCTNNB1#4
isgCTNNB1#2
isgMYC#1
isgMYC#2
Tumor volume / mm3
1200
1000
800
600
400
200
0
-7
0
7
14
21
28
35
42
49
Days of dox treatment
E
H&E
GFP
β-catenin
Ki67
200 µm

Figure 6

Figure 6. *RNF43*/*FBXW7*-double mutant cancer cells lost dependence on β-catenin.

(A, B) Knockdown of *CTNNB1* or *MYC* in *FBXW7*-wildtype HPAF-II cells and the effects on tumor growth. **(A)** HPAF-II cells stably expressing dCas9-KRAB were transduced with a doxycycline-inducible sgRNA expression vector targeting *CTNNB1* or *MYC* promoters with two independent sgRNAs per gene, or a non-targeting control (isgNTC#2). These cells were treated with doxycycline for 4 days, followed by RT-qPCR analysis. **(B)** These cells without doxycycline treatment were subcutaneously injected into NSG mice. After tumor establishment, mice were put on continuous doxycycline feed until the end of the study. Data are represented as mean + SEM (n = 6 tumors/arm).

(C, D) Knockdown of *CTNNB1* or *MYC* in *FBXW7*-mutant HuCCT1 cells and the effects on tumor growth. Experiments were performed as in **(A, B)**. **(D)** Data are represented as mean + SEM (n = 6-8 tumors/arm).

(E) HuCCT1 cells retained spontaneous metastatic capability after β-catenin knockdown. Representative images of H&E, GFP, β-catenin, and Ki67 staining of a lung metastasis (out of more than 10 metastatic lesions per lung section) from a mouse with the HuCCT1 isgCTNNB1#4 subcutaneous tumor. The sgRNA-expressing vector also expressed GFP, which was stained to distinguish the cancer cells from the host tissues.

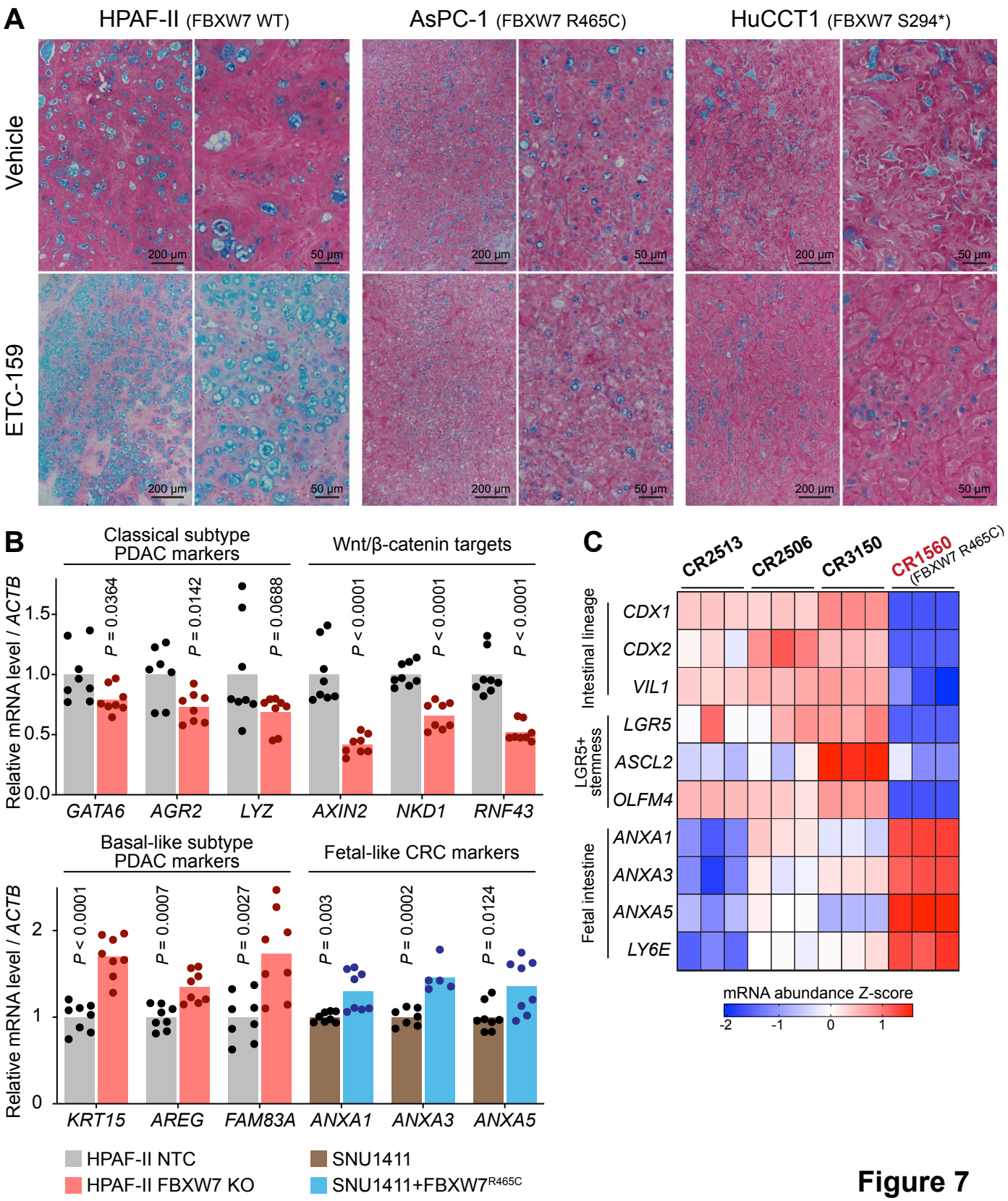
A
HPAF-II (FBXW7 WT)
AsPC-1 (FBXW7 R465C)
HuCCT1 (FBXW7 S294*)
Vehicle
ETC-159
200 µm
50 µm
B
Classical subtype PDAC markers
Wnt/β-catenin targets
Relative mRNA level / ACTB
P = 0.0364
P = 0.0142
P = 0.0688
P < 0.0001
P < 0.0001
P < 0.0001
GATA6
AGR2
LYZ
AXIN2
NKD1
RNF43
Basal-like subtype PDAC markers
Fetal-like CRC markers
P < 0.0001
P = 0.0007
P = 0.0027
P = 0.003
P = 0.0002
P = 0.0124
KRT15
AREG
FAM83A
ANXA1
ANXA3
ANXA5
HPAF-II NTC
HPAF-II FBXW7 KO
SNU1411
SNU1411+FBXW7R465C
C
CR2513
CR2506
CR3150
CR1560 (FBXW7 R465C)
Intestinal lineage
CDX1
CDX2
VIL1
LGR5+ stemness
LGR5
ASCL2
OLFM4
Fetal intestine
ANXA1
ANXA3
ANXA5
LY6E
mRNA abundance Z-score
-2
-1
0
1

Figure 7

Figure 7. Inactivation of FBXW7 is associated with dedifferentiation and phenotypic switching in *RNF43*-mutant/*RSPO*-fusion cancers.

(A) *RNF43*/*FBXW7*-double mutant cancer xenografts were resistant to Wnt inhibition-induced differentiation. Alcian blue (pH 2.5) mucin staining was performed on tumor samples treated with vehicle or ETC-159 **(Fig. 2B)**.

(B) Inactivation of FBXW7 promoted molecular subtype switching in *RNF43*-mutant pancreatic tumors and *RSPO3*-fusion colorectal tumors. mRNA abundance of the indicated marker genes was measured in HPAF-II and SNU1411 xenografts. Four independent tumors per group were analyzed by RT-qPCR with technical replicates for each sample. *P* values of 2-tailed, unpaired *t* test are shown.

(C) Among the *RSPO3*-fusion colorectal cancer PDXs **(Fig. 2C),** the *FBXW7*-mutant PDX was dedifferentiated and showed fetal-like colorectal cancer features. mRNA abundance of the indicated marker genes was extracted from GSE73906 and shown as Z-score.

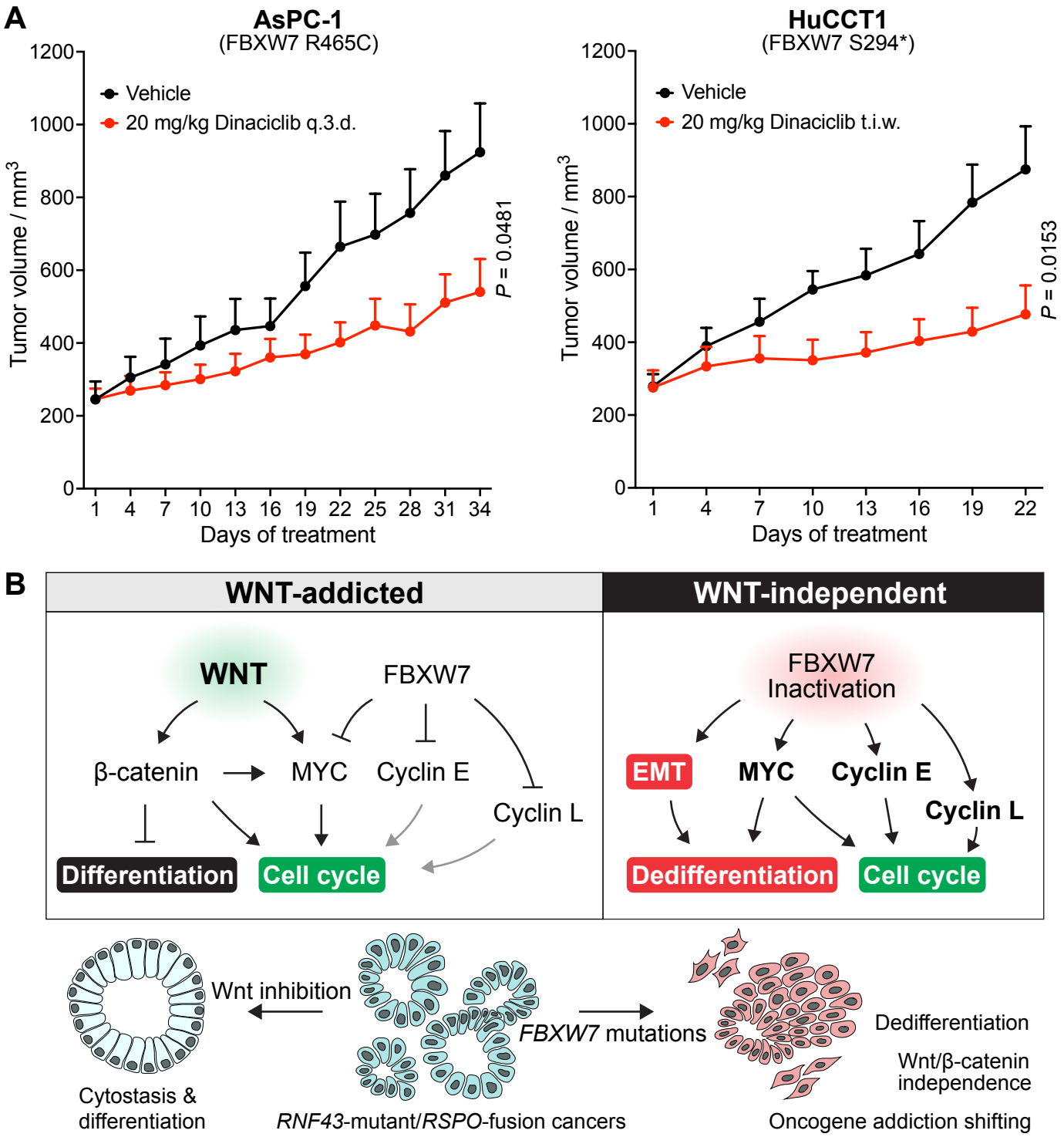
A
AsPC-1
(FBXW7 R465C)
Vehicle
20 mg/kg Dinaciclib q.3.d.
Tumor volume / mm3
Days of treatment
P = 0.0481
HuCCT1
(FBXW7 S294*)
Vehicle
20 mg/kg Dinaciclib t.i.w.
Tumor volume / mm3
Days of treatment
P = 0.0153
B
WNT-addicted
WNT-independent
WNT
FBXW7
β-catenin
MYC
Cyclin E
Cyclin L
Differentiation
Cell cycle
FBXW7
Inactivation
EMT
MYC
Cyclin E
Cyclin L
Dedifferentiation
Cell cycle
Wnt inhibition
FBXW7 mutations
Dedifferentiation
Wnt/β-catenin
independence
Cytostasis &
differentiation
RNF43-mutant/RSPO-fusion cancers
Oncogene addiction shifting

Figure 8

Figure 8. *RNF43*/*FBXW7*-double mutant tumors are sensitive to multi-CDK inhibition.

(A) The multi-CDK inhibitor dinaciclib significantly inhibited *RNF43*/*FBXW7*-double mutant tumor growth. AsPC-1 or HuCCT1 cells were injected subcutaneously into NSG mice. After tumor establishment, mice were treated with vehicle or 20 mg/kg dinaciclib once every three days (q.3.d.) or three times a week (t.i.w.). Data are represented as mean + SEM (n = 6-8 tumors/arm). *P* values of 2-tailed, unpaired *t* test between vehicle and dinaciclib arms at the last time point are shown.

(B) Schematic model of FBXW7 inactivation-caused Wnt independence and dedifferentiation in *RNF43*-mutant/*RSPO*-fusion cancer. Please refer to the text for detailed description.